ISTANBUL TECHNICAL UNIVERSITY ★ GRADUATE SCHOOL OF SCIENCE ENGINEERING AND TECHNOLOGY

AERODYNAMIC ANALYSES AND DESIGN OPTIMIZATION OF A C- SHAPED WING

M.Sc. THESIS

Hulya SUKAS

Department of Aerospace and Aeronautical

Aerospace and Aeronautical Engineering Programme

Thesis Advisor: Prof. Dr. Melike NIKBAY

MAY 2019

ISTANBUL TECHNICAL UNIVERSITY ★ GRADUATE SCHOOL OF SCIENCE ENGINEERING AND TECHNOLOGY

AERODYNAMIC ANALYSES AND DESIGN OPTIMIZATION OF A C- SHAPED WING

M.Sc. THESIS

Hulya SUKAS
(511161175)

Department of Aerospace and Aeronautical Engineering

Aerospace and Aeronautical Engineering Programme

Thesis Advisor: Prof. Dr. Melike NIKBAY

MAY 2019

İSTANBUL TEKNİK ÜNİVERSİTESİ ★ FEN BİLİMLERİ ENSTİTÜSÜ

C-TİPİ KANAT KONFİGURASYONUNUN AERODİNAMİK ANALİZLERİ VE DİZAYN OPTİMİZASYONU

YÜKSEK LİSANS TEZİ

Hülya SUKAS
(511161175)

Uzay ve Uçak Mühendisliği Anabilim Dalı

Uçak ve Uzay Mühendisliği Programı

Tez Danışmanı: Prof. Dr. Melike NIKBAY

MAYIS 2019

Hulya SUKAS, a M.Sc. student of ITU Graduate School of Science Engineering and Technology student ID 511161175, successfully defended the thesis/dissertation entitled "AERODYNAMIC ANALYSES AND DESIGN OPTIMIZATION OF A C-SHAPED WING", which she prepared after fulfilling the requirements specified in the associated legislations, before the jury whose signatures are below.

Thesis Advisor :   **Prof. Dr. Melike NIKBAY**   ....
İstanbul Technical University

Jury Members :   **Prof. Dr. Mehmet SAHIN**   ....
Istanbul Technical University

    Prof. Dr. Mehmet A.AKGUN   ....
Yeditepe University

Date of Submission : 03 May 2019
Date of Defense   : 14 June 2019

To my husband Omer Faruk,

FOREWORD

First of all, I would like to thank my supervisor Prof. Dr. Melike NIKBAY who supported me throughout my graduate studies and master thesis. Her experience and academic achievements have been a guide for me to complete my studies.

Secondly, I would like to thank Prof. Dr. Mehmet SAHIN. I took very benefical courses from him and I have gained lots of coding abilities during projects of his lectures.

Also, I would like to thank my colleague, Berkay PIRLEPELI for his help during the optimization section of this study.

Finally, I would like to thank my family and especially my husband for his patience and support during my master education.

May 2019   Hulya SUKAS
(Ocean Engineer, Mechanical Engineer)

TABLE OF CONTENTS

ABBREVIATIONS

AoA	**:** Angle of Attack
BL	**:** Boundary Layer
CAD	**:** Computer Aided Design
CFD	**:** Computational Fluid Dynamics
CSD	**:** Computational Structural Dynamics
DGM	**:** Discontinous Galerkin Method
DNS	**:** Direct Numerical Simulations
FDM	**:** Finite Difference Method
FEM	**:** Finite Element Method
FVM	**:** Finite Volume Method
GUI	**:** Guide User Interface
LES	**:** Large Eddy Simulations
LHS	**:** Latin Hybercube Sampling
NASA	**:** National Aeronautics and Space Administration
PDE	**:** Partial Differential Equation
RANS	**:** Reynolds Averaged Navier Stokes
SEM	**:** Spectural Element Method
LHS	**:** Latin Hypercube Sampling
V&V	**:** Verification and Validation

SYMBOLS

C_L	: Lift coefficient.
C_D	: Drag coefficient.
C_G	: Correction factor
$\vec{d}$	: Direction vector.
E	: Experimental result.
N_s	: Number of sampling.
P	: Pressure
p_G	: Order of accuracy
r	: Grid refinement ratio.
Re	: Reynolds number.
R_G	: Grid convergence ratio.
s_1	: Fine mesh result.
s_2	: Medium mesh result.
s_3	: Coarse mesh result.
S_L	: Lower value of the simulation.
S_U	: Upper value of the simulation.
U_D	: Total experimental uncertainty.
U_G	: Grid uncertainty.
U_{GC}	: Corrected grid uncertainty.
u	: Velocity component at x direction.
v	: Velocity component at y direction.
w	: Velocity component at z direction.
$z_i(x)$	: Wellknown points.
ϑ	: Kinematic viscosity.
λ	: Weighting factor.
σ	: Variance.
σ_K	: Kriging variance
μ	: Lagrange multiplier.
α_K	: Step size.

ρ	:	Density of air.
τ	:	Shear stress.
ε_{21}	:	Difference between medium and fine mesh results.
ε_{32}	:	Difference between coarse and medium mesh results.
δ	:	Kronecker's delta.
δ_{RE}^{*}	:	Numerical error.
δ_{SN}	:	Numerical error.
l_m	:	Mixing length model.
u^*	:	Friction velocity.
δ_{BL}	:	Boundary layer thickness.
$y+$	:	Non dimensional distance from the wall.
ϕ	:	Dihedral angle of C-wing geometry.

LIST OF TABLES

LIST OF FIGURES

AERODYNAMIC ANALYSES AND DESIGN OPTIMIZATION OF A C-SHAPED WING CONFIGURATION

SUMMARY

Increasing fuel prices and environmental pollution due to fuel consumption require immediate improvements in aerodynamic/hydrodynamic performance of air, sea and land vehicles. In this context, it can be said that fuel consumption is directly related to the drag force acting on the aircraft. Researchers have tried to enhance aerodynamic properties of air vehicles so far by optimizing the designs in order to reduce drag force. This study investigates the aerodynamic efficiency (C_L/C_D) of a specific non-planar wing configuration (C-shaped wing). Lift and drag coefficients are predicted numerically using a RANS based Computational Fluid Dynamics (CFD) approach and the results obtained were compared for a range of angle of attacks.

A computational framework is established to carry out aerodynamic flow analyses in coordination with other tools to enable design optimization. The optimization workflow employs four main tools; an open source optimization tool Dakota whis was developed in the Sandia National Laboratory is used as optimization driver, OpenVSP is utilized to generate a parametric model of the geometry, Pointwise is used for grid generation in computational flow domain and StarCCM + is used to perform aerodynamic flow analyses. In addition, some supplementary scripts are developed in Python and Java to couple the interacting tools and enable an automatic flow for optimization process.

Aerodynamic flow analyses are performed at certain AoAs (Angle of Attacks) to see the accuracy of present physical model for both planar and C-wing configurations. The numerical results obtained is compared with the experimental data conducted at Glasgow University. A verification and validation study is also performed to investigate the effect of number of grid elements on the numerical results to quantify the CFD work.

Since optimization process requires function evaluations for the optimization criteria for many times, CFD based high-fidelity flow solutions increase the time needed to finalize the optimization enormously. Then as a remedy, surrogate modelling can be used to during the optimization process to represent the high fidelity solution by a low fidelity solution which is constructed based on a finite set of sampling data received from the high fidelity solution.

To create the sampling data, Latin Hypercube Sampling method is used to select the random variation of the chosen optimization variable in the design space. Using these results, a surrogate model was created by Kriging Method. The drag and lift force results were recorded as the outputs of simulations to be used as optimization objectives. For the optimization procedure, Conjugate Gradient Method and Quasi Newton Method (Broyden–Fletcher–Goldfarb–Shanno and Finite Difference Method) were used in Dakota.

In this thesis, three optimization variables defining C-wing configuration are selected and optimum wing geometries are obtained for maximizing the objective function (C_L/C_D) value with a given geometric constraint.

C-TİPİ KANAT KONFİGURASYONUNUN AERODİNAMİK ANALİZLERİ VE DİZAYN OPTİMİZASYONU

ÖZET

Havacılık endüstrisinde, en küçük verim kayıpları bile yakıt tüketiminde yıllık olarak milyonlarca liraya karşılık gelmektedir. Airbus'ın yapmış olduğu araştırmalara göre, büyük bir nakliye uçağı için sürükleme kuvvetindeki % 1'lik düşüş yaklaşık olarak 400.000 litrelik yakıt tasarrufuna karşılık gelmekte ve bunun sonucu olarak da yılda ortalama 5000 kg zararlı emisyon gazlarının atmosfere salınımı önlenmektedir [1]. Buradan hareketle, yapılacak olan yeni tasarımlarda ekonomik ve çevresel olarak eşdeğer bir performans elde edilmeye çalışılmalıdır. Bunu gerçekleştirebilmek için ilk olarak uçağın hareketine karşı oluşacak sürükleme kuvveti kanat ve/veya kanatçık geometrileri optimize edilerek azaltılmalıdır.

Bilindiği üzere uçuş esnasında kanatların alt kısmında yüksek basınç, üst kısmında ise düşük basınç alanı oluşur ve hava akışı da her zaman yüksek basınç alanından düşük basınç alanına doğru hareket edeceğinden, kanat geometrisi sebebi ile kanat ucu girdapları oluşur ve bu girdaplardan dolayı artan sürükleme etkisine indüklenmiş sürükleme kuvveti denir. İndüklenmiş sürükleme kuvveti kanadın maksimum taşıma kuvvetini azaltacağı gibi aynı zamanda uçağa etkiyen sürükleme kuvvetini dolayısıyla yakıt tüketimini arttırır. Seyir esnasında uçağa etkiyen toplam sürükleme kuvvetinin yaklaşık %40'ını indüklenmiş sürükleme kuvvetinin oluşturduğu bilinmektedir [2]. İndüklenmiş sürükleme kuvveti kanat ucu geometrisinden önemli ölçüde etkilenmektedir.

Ticari havacılıkta, büyük nakliye uçaklarının ardında oluşan güçlü kanat ucu girdapları yakıt verimsizliğine sebep olduğu kadar aynı zamanda uçuş güvenliği açısından oldukça tehlikelidir. Bu nedenle, yakıt tasarrufu amacıyla girdapları azaltacak olan bir yenilik, uçaklar arasındaki girdap kaynaklı etkileşimlerden doğabilecek olumsuzlukları da minimize edecektir. Ayrıca girdapların minimize edilmesiyle yeni havalanmış olan bir uçağın izinin kaybolması için beklenen süre kısaltılabilirse, havalimanlarından belirli süre içerisinde havalanabilen uçak sayısında artış olması sağlanacaktır.

Düzlemsel olmayan kanat geometrilerinde yapılan yenilikler 1950'lerden bu yana uçak tasarımındaki birkaç önemli değişiklikten birini temsil etmektedir. Düzlemsel olmayan kanatlar, aynı açıklık ve taşıma kuvvetine sahip düzlemsel kanatlara kıyasla daha düşük sürükleme kuvveti oluşmasını sağlarlar. Klasik tasarıma sahip bir kanadın ucunda kanatçık (winglet) olmadığından akım bozulması sebebi ile girdaplar ve indüklenmiş sürükleme kuvveti meydana gelmektedir. Aynı kanat üzerine kanatçık (winglet) eklendiğinde burada oluşan akım bozulmaları azaldığından girdaplar da azalmakta ve dolayısı ile sürükleme kuvvetinde düşüş gözlenmektedir.

Kanat ucu girdaplarını azaltmaya yönelik tasarlanan kanat tiplerinden bir diğeri de kapalı yüzeyli (closed lifting surface) kanat tipleridir. Buna örnek olarak kutu-kanat (box-wing) tipinin incelendiği bir çalışmada belirli bir kanat açıklığı, taşıma kuvveti

ve irtifada kutu-kanatların en düşük indüklenmiş sürükleme kuvvetini ürettiği gözlemlenmiştir. C-kanatları (C-wings) ise klasik düşey kanatçıkların üzerine, küçük boyutlu yatay kanatçıklar eklenerek elde edilen tasarımlardır. Fiziksel olarak kutu-kanat tasarımının farklı bir kombinasyonu olarak düşünülebilir. Jansen ve Kroo'nun [3,4] çalışmalarında C-kanatların, klasik düşey tipteki kanatçıkların olduğu kanatlara göre aerodinamik performansı arttırıcı bir potansiyele sahip olduğunu belirtilmiştir. Yapılan çalışmalar neticesinde tasarım olarak kutu-kanat konfigürasyonuna yaklaşıldıkça indüklenmiş sürükleme kuvvetinde azalma olduğu gözlemlenmiştir [3,4]. İlk etapta kanat ağırlığını arttıracak olan bu kanatçıkların tasarımda ekstra yüzeyler olacağı ve tercih edilmeyeceği düşünülse de bu artışa rağmen bu ekstra yüzeylerin girdapları azaltarak sürükleme kuvvetini dolayısıyla da yakıt sarfiyatını önemli ölçüde azalttığı görülmüştür.

Sonuç olarak bir hava aracının kanat geometrisinde yapılan değişiklikler ile yakıt tüketiminin azaltıldığı ve uçuş veriminin arttırıldığı saptanmıştır. Kanat uç geometrisinin değiştirilmesiyle yeniden tasarlanacak olan düzlemsel olmayan kanat sistemlerinin aerodinamik verimlerinin iyileştiği görülmüştür. Düzlemsel olmayan kanat tasarımları, klasik tipteki kanat ucuna sadece kanatçık eklenerek yapılabileceği gibi kanadı kutu şeklinde tasarlayarak da elde edilebilir. Bu doğrultuda tasarlanabilecek düzlemsel olmayan kanat çeşitlerinden biri olan C-kanat tipi, kutu kanat tasarımlarının konfigürasyonu olarak düşünülebilir. C-kanadın tasarım sürecinde minimum sürükleme kuvvetini yada maksimum aerodinamik verimi elde edebilmek için belirli kısıtlamalar ve tasarım değişkenleri göz önüne alınarak bir optimizasyon çalışması yapılmasına ihtiyaç duyulmaktadır.

Bu tezde nihai hedef düzlemsel olmayan kanatlar üzerinde yer alacak olan kanatçıkların aerodinamik performans açısından incelenmesi ve optimum özelliklerde bir C tipi kanatçık tasarlanmasıdır. Elde edilen sonuçlara göre hava aracının maliyet, güvenilirlik, performans, yakıt tüketimi gibi parametrelerinde iyileşmeler görülmesi beklenmektedir.

Bu bağlamda aerodinamik akış analizlerinin yapıldığı bir sistemin, optimizasyon aracı ile bağlaşık bir şekilde çalışması gerekmektedir. Bu tezde kurulan optimizasyon çatısı temelde dört ana programı otomatik olarak çalıştırmaktadır. Optimizasyon sürücüsü olarak Sandia Ulusal Labaratuarında geliştirilen açık kaynaklı "Dakota" programı, parametrik geometrinin modellenmesi için NASA'nın açık kaynaklı aracı olan "OpenVSP", akış hacmi ağ elemanlarının oluşturulması için Pointwise ve akış analizlerini gerçekleştirebilmek için StarCCM+ programları kullanılmıştır. Bu araçların birbirleri ile haberleşebilecek bir şekilde çalışması için gerekli betikler Python ve Java dillerinde yazılmıştır.

Kurulan fiziksel modelin doğruluğunu görebilmek için belirli hücum açılarında düzlemsel ve düzlemsel olmayan C-kanat geometrileri için akış analizleri yapılmış ve Glasgow Üniversitesinde yapılmış rüzgar tüneli deney sonuçları ile karşılaştırılmıştır. Sonuçların kabul edilebilir bir hata yüzdesi ile tahmin edildiği görüldükten sonra ağ elemanlarının sonuçlara etkisini incelemek için doğrulama ve sağlama çalışması yapılmış ve optimum ağ elemanları parametreleri belirlenmiştir. Fiziksel modelin doğruluğundan emin olunduktan sonra bu model kullanılarak optimizasyon çalışmaları yapılmıştır.

Yüksek doğrulukta CFD çözümleri temel alınarak yapılan optimizasyon çalışmaları hesaplama zamanını artırmaktadır. Bu yüzden yüksek doğruluklu çözümlemeyi temsil

eden ve rastgele seçilen değişkenlerden oluşan örnekleme kümeleri ile elde edilen vekil model kullanılmıştır.

Vekil modelin oluşturulması sürecinde ilk olarak "Latin Hiperküp Örnekleme"si kullanılarak rastgele seçilen değişkenler ile akış analizleri yapılmış, taşıma (lift) ve sürükleme (drag) kuvveti sonuçları kaydedilmiştir. Bu sonuçlar kullanılarak "Kriging Metodu" ile vekil model oluşturulmuştur. Böylece belirlenmiş olan aralıkta yeni bir değişkene ait sonuç merak edildiğinde tekrar analiz yapmak yerine bu modelden sonuç alınabilmiştir. Vekil model oluşturulduktan sonra verilen aralıktaki değişkenler için optimizasyon sürecine geçilmiştir. Optimizasyon çalışması için Dakota'da bulunan "Eşlenik Gradyan Metodu" ve "Yarı-Newton Metodları (Broyden–Fletcher–Goldfarb–Shanno ve Sonlu Farklar Metodu)" kullanılmıştır.

Bu tezde C tipi kanat uç geometrisine ait üç farklı değişken belirlenmiş, verilen sınırlarda ve kısıtlamalar altında optimum geometri aranmıştır. Amaç fonksiyonu olarak ise (C_L/C_D) değeri maksimize edilmeye çalışılmıştır. Elde edilen sonuç geometrisinin orjinal geometriye göre daha fazla taşıma ve daha az sürükleme kuvvetine sahip olduğu görülmüş ve aerodinamik açıdan daha verimli bir geometri elde edilmiştir.

1. INTRODUCTION

Researchers around the world have made various shape optimizations to reduce the fuel consumption of air vehicles. It has been shown that non-planar wing systems have some benefits on aerodynamic performance compared to traditional wings. For this reason, many new configurations have been produced and developed so far. In order to improve the aerodynamic performance of these designs, a framework which includes numerical methods and optimization drivers must be implemented.

1.1 Purpose of Thesis

In this thesis, shape optimization of a non-planar wing has been performed to increase its aerodynamic efficiency. In this context, aerodynamic characteristics of C-wing configurations were investigated. In the first phase of the thesis, validation of the numerical model was done for planar wing geometry and also an initial C-wing configuration with various angle of attacks using the Skinner's [5] experimental data. In the second step, aerodynamic optimization of the initial C-wing geometry has been carried out for the three selected design variables of the geometry using three different optimization approach. In order to perform this optimization process, an algorithm which connects the pre-processing and flow solver was used and these calculations were done automatically within the optimization framework. For this reason, aerodynamic flow analyses and shape optimization process were run together in a loop utilizing the codes developed.

1.2 Literature Review

Increasing fuel prices and environmental pollution due to fuel consumption requires immediate improvements in aerodynamic/hydrodynamic performance of air, sea and land vehicles. In this context, it can be said that fuel consumption is directly related to the drag force acting on the aircraft. So far, researchers have tried to enhance

aerodynamic properties of air vehicles by optimizing the shape of body in order to reduce drag force.

The Airbus company has showed that 1% reduction in drag force of the A340 aircraft saved 400,000 liters of fuel per year and prevented 5000 kg of emissions released into the atmosphere [1]. Approximately 40% of the drag force is composed of induced drag force, ie. vortex-drag [2]. As the air moves from the high pressure zone to the low, the vortices occur at the wing tips because of the geometrical shape of wing and this will generate induced drag force around wing tips. These vortices can to be reduced with the usage of non-planar wing configurations by changing the form of wing tips. The design of non-planar wing systems can be achieved by adding only winglets to traditional form as well as also adding several parts shown in Figure 1.1.

Figure 1.1. Various types of non-planar wing configurations used in aircrafts [6].

Figure 1.2 shows different types of wing geometries that are considered for fixed total lift and span. These designs are compared in terms of span efficiency (η) which is defined as the ratio of induced drag of planar wing to that of non-planar wing.
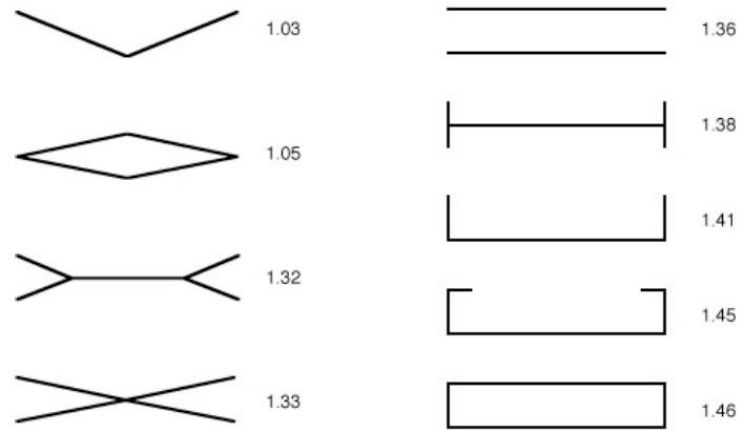
Figure 1.2. Span efficiency of non-planar wings. [13]

According to Kroo [5], the box-wing designs have the highest span efficiency (1.46) among these nine different configurations shown in Figure 1.2. Recently, a great deal of attention has been attracted to aerodynamic performance of box-wing geometries. Andrews and Perez [6] investigated the performance of box wing and traditional wing designs for representative regional-jet missions. In their study, although the ratio of lift and drag force was found to be quite low for box-wings in preliminary design, it was shown that the fuel required to carry these wings causes an increase about 1-5%. However, it was concluded that the box-wing configurations are better than conventional planar wing designs in terms of aerodynamic performance, if fuel consumption is restricted. Hicken and Zingg [2] used an Euler equation-based algorithm to perform optimization studies for non-planar wings. They showed that a nonplanar split-tip configuration outperforms both the winglet and box-wing geometries for the same spanwise and vertical bound constraints as the maximization of the vertical extent at the tip can be more easily.

In order to achieve more accurate results in aerodynamic performance studies, structural interactions must be included in the problem. Jansen et. al. [3] have made a multi-disciplinary approach for the non-planar wing systems in terms of aerodynamic, structural and aero-structure. They used panel method and equivalent-beam FEM method for their analyses. Aerodynamic optimization and multi-disciplinary aero-structural optimizations were performed using Lagrangian particle swarm method. As a result, they figured out that enclosed surfaces such as box-wing or joined wing are optimum designs if wing systems are examined only aerodynamically. However,

3

winglet designs are said to be optimal in terms of induced (vortex) drag when aero-structural approach is considered.

Although the aerodynamic efficiency increases as we approach the box-wing design, the production costs and the mass increment of the geometry are disadvantageous. For this reason, C-wing geometries are stated as the second best wing type for span efficiency as depicted in Figure 1.2. C-wings can be considered as a different combination of box-wing design and can be obtained by adding horizontal winglets to classic type vertical winglets as shown in Figure 1.3.
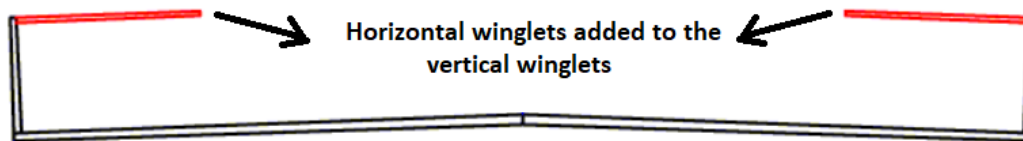
Figure 1.3. A profile view of C-wing with its vertical and horizontal winglets.

Suresha et al. numerically showed that C-wings were more efficient compared to planar wings in terms of aerodynamic performance for a certain range of angle of attacks [7]. They also investigated the effect of mounting angle of C-wing geometry on lift and drag forces and obtained optimum mounting angle. Gobpinaath et al. carried out not only CFD method but also conduct experiment for four different C-wing geometries of Airbus A300 and demonstrated that induced drag force obtained is lower than that of the planar wing system [8]. Peng and Jinglong [9] investigated aeroelastic features of C-wing using high fidelity analysis methods. Euler flow equations was solved during the numerical analyses and structural vibration was investigated using computational structure dynamics (CSD) . Features of flutter and limit cycle oscillation of the C-wing geometry were obtained and the numerical outputs were compared with the experimental data. Another study [10] about C-wing configuration is the usage of Euler-Lagrange integral equations to obtain circulation distribution for several non-planar wing types including C-wing shape. In their study, the analytical method used is based on Munk's studies [25]. The primary goal of their study was to obtain maximum aerdynamic efficiency for the C-wings and they validated the numerical results obtained with thebenchmark cases in literature.

Designing C-wing geometry can affect the maneuverability of aircrafts as it changes the point of pitching moment. Ning and Kroo [11] investigated optimization of C-wing in terms of manevuring ability for an aircraft without tail. As a result of their study,

they stated that using C-wings may be beneficial for aircrafts without tail with nose up pitching moment about the aerodynamic center. Skinner and Behtash [12] also performed wind tunnel experiments for planar and C-wing configurations and they obtained a lower induced drag force for C-wing compared to planar wing design.

In this study, first RANS based numerical simulations of planar and non-planar (C-wing) designs were carried out using the same aircraft geometry used in [12] and the results obtained were validated with the wind tunnel experiment data. Subsequently, an optimization procedure was implemented to the C-wing geometry for further to increase aerodynamic efficiency under certain constraints.

1.3 Hypothesis

The purpose of this thesis is to investigate the optimum C-wing configuration in order to generate maximum aerodynamic efficiency. Therefore, it is essential to ensure the accuracy of physical setup of numerical model in flow simulations. The numerical method was first verified using the wind tunnel results which includes lift and drag forces. After the numerical model was found to be working correctly, optimization process by using optimization variables was carried out.

2. NUMERICAL METHOD

In this thesis, a Reynolds Averaged Navier Stokes (RANS) based Computational Fluid Dynamics (CFD) approach was used to calculate the flow field properties around the body. CFD is a branch of fluid mechanics that solves problems using numerical analyses and data structures. Fundamentally, CFD methods such as Finite Difference Method (FDM), Finite Element Method (FEM), Finite Volume Method (FVM), Spectral Element Method (SEM), Discontinous Galerkin Method (DGM) etc. convert any partial differential equations into algebraic form. These methods can be used in a wide range of application areas, e.g. aerospace and marine industries, car and sport aerodynamics, enviromental, biomedical or nuclear reactor problems. For fluid flows, Figure 2.1 indicates the mathematical models used in CFD and its sub-sections. In this thesis, Navier Stokes equations based on continuum model were solved to obtain velocity and pressure fields around the wing.
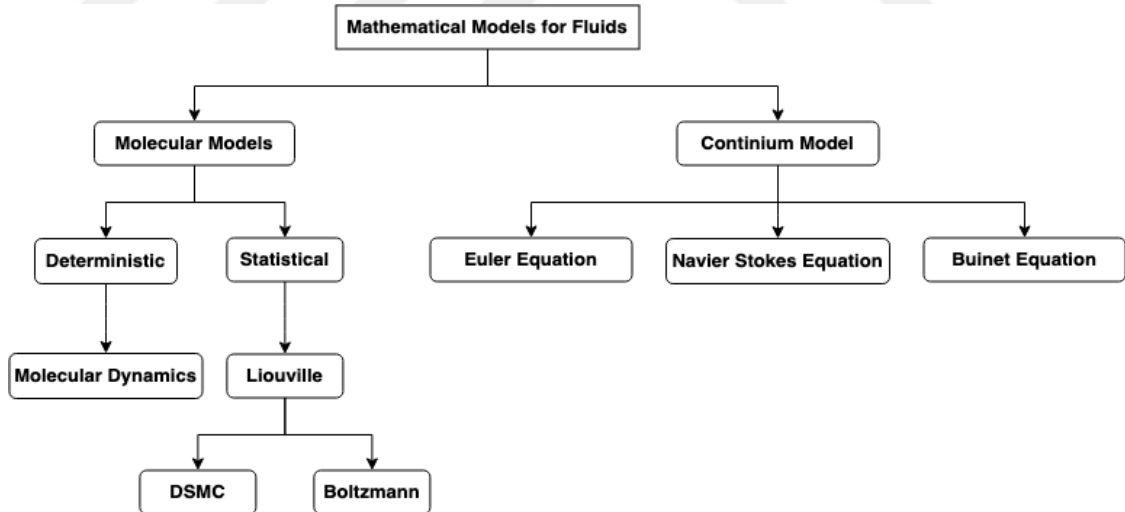
Figure 2.1. A scheme of mathematical models for fluids.

Solution of Navier-Stokes equations will be explained in detail in the next subsections. According to Figure 2.1, CFD methods can be implemented by using two types of approach; inviscid and viscous methods. Inviscid methods are generally based on potential theory, thus Euler equation is considered as the conservation equation. However, viscous effects should be included in the problem for a more realistic

solution. It is possible to see the effect of boundary layer, turbulence and wake for a given problem with the viscous approach. Since a numerical validation of the experimental results will be carried out in this study, viscous effects should be included. In fluid mechanics problems, we need to solve basic equations such as conservation of mass and momentum to obtain pressure and velocity fields around any geometry. The momentum equations are generally called as Navier-Stokes equations, while the mass conservation equation is known as continuity equation. In this thesis, we neglect the compressibility as the velocity of air is sufficiently low (M=0.145). Therefore, the 3-D incompressible Navier-Stokes equations (2.1,2.2,2.3) and the continuity equation (2.4) can be written in the cartesian coordinate system for x, y and z directions as follows:

$$Re\frac{\partial u}{\partial t} + Re\frac{\partial(uu)}{\partial x} + Re\frac{\partial(uv)}{\partial y} + Re\frac{\partial(uw)}{\partial z} = -\frac{\partial P}{\partial x} + \frac{\partial^2 u}{\partial x^2} + \frac{\partial^2 u}{\partial y^2} + \frac{\partial^2 v}{\partial z^2} \quad (2.1)$$

$$Re\frac{\partial v}{\partial t} + Re\frac{\partial(uv)}{\partial x} + Re\frac{\partial(vv)}{\partial y} + Re\frac{\partial(vw)}{\partial z} = -\frac{\partial P}{\partial y} + \frac{\partial^2 v}{\partial x^2} + \frac{\partial^2 v}{\partial y^2} + \frac{\partial^2 v}{\partial z^2} \quad (2.2)$$

$$Re\frac{\partial w}{\partial t} + Re\frac{\partial(wv)}{\partial x} + Re\frac{\partial(wv)}{\partial y} + Re\frac{\partial(ww)}{\partial z} = -\frac{\partial P}{\partial z} + \frac{\partial^2 v}{\partial x^2} + \frac{\partial^2 v}{\partial y^2} + \frac{\partial^2 v}{\partial z^2} \quad (2.3)$$

$$\frac{\partial u}{\partial x} + \frac{\partial v}{\partial y} + \frac{\partial w}{\partial z} = 0 \quad (2.4)$$

The equation system above represents the flow around any geometry and should be solved together to obtain pressure and velocity fields. However, the main point is here that these coupled partial differential equations (PDE) cannot be solved analytically. Hence we need to utilize numerical methods such as FDM, FEM and FVM. In this study, FVM was selected to convert PDE into algebraic form to solve the equations in the computational domain.

The equations given above are valid for laminar flows. However, several different numerical models can be used to solve conservation equations when the flow is turbulent. Some of widely used models can be sorted as Direct Numerical Simulation (DNS), Large Eddy Simulation (LES) and Reynolds Avarged Navier Stokes Equations (RANS).

2.1 Numerical Models for Flow Simulations

2.1.1 Direct numerical simulations (DNS)

Using DNS method, it is possible to obtain all information within the flow area without any modeling. Therefore, mesh size must be extremely large even in very low Reynolds numbers. Although it is the most accurate method than the rest, it is the most expensive approach in terms of computational power due to essential usage of high mesh quality [15].

2.1.2 Large eddy simulations (LES)

In terms of computational resource, LES method can be assumed as an approach between RANS and DNS approaches. The primary goal of usage of LES method is to reduce computer source needed by modeling small scales in analyses instead of direct solution [15].

2.1.3 Reynolds Avareged Navier Stokes (RANS)

In RANS method, all quantities of flow are modeled from large scale to the small scales. It can be considered as the cheapest method in terms of computational time compared to LES and DNS. The governing equations are transformed by time-averaged forms and the turbulence fluctuations are modeled. The RANS method is explained in detail in the next subsection [15].

The comparison of these three numerical models can be briefly explained with the following figures. Figure 2.1 shows the conceptual spectrums of these methods. It can be clearly seen that, the grey part of the spectrums can be simulated, whereas the remaining part (white) is modelled. Since modelling is a kind of prediction, thus accuracy will be lower comparing with those of the simulated types.
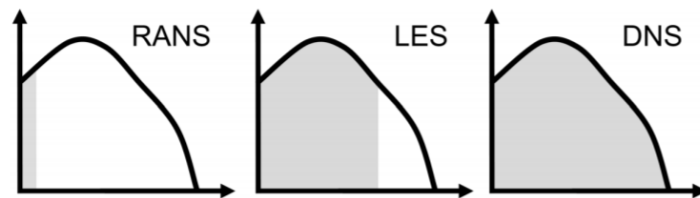
Figure 2.2. Comparison of the numerical models in terms of the ability of simulated (grey) and modelled (white) [34].

It can be seen from Figure 2.2. RANS simulations captures only the large scale informations while DNS can caprture all scales of informations in the flow.
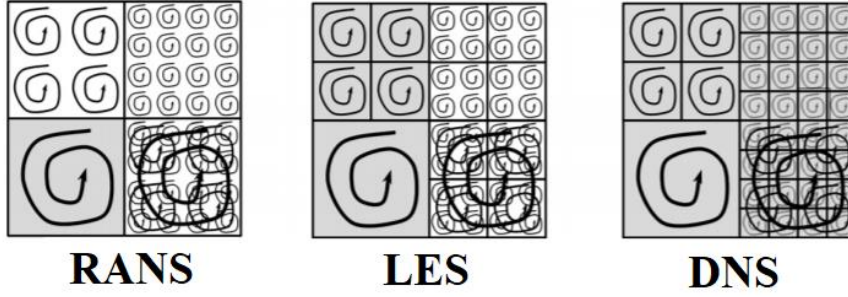
Figure 2.3. The abilities of the models to capture large and small scales [34].

2.1.3.1 Derivation of RANS equations

The instant values in flow area can be obtained when the time-averaging is applied to the basic conservation equations. Time-averaged calculation for any physical size is given as:

$$Q = \frac{1}{T}\int_{t_0}^{t_0+T} Q(t)dt \tag{2.6}$$

where T represents the time interval. The instantaneus velocity components (u_1, u_2, u_3) and the pressure (p) of the flow are defined in equation 2.7 in terms of mean components $(\bar{u}_1, \bar{u}_2, \bar{u}_3, \bar{p})$ and flactuations (u_1', u_2', u_3', p').

$$
\begin{aligned}
u_1 &= \bar{u}_1 + u_1' \\
u_2 &= \bar{u}_2 + u_2' \\
u_3 &= \bar{u}_3 + u_3' \\
p &= \bar{p} + p'
\end{aligned}
\tag{2.7}
$$

The RANS equations in tensor form given in equation 2.8 are obtained by substituting instantaneous velocity and pressure terms in conservation equations.

$$\frac{D\bar{V}}{Dt} + \frac{\partial}{\partial x_j}\left(\overline{u_i'u_j'}\right) = g - \frac{1}{\rho}\nabla\bar{p} + \frac{\partial}{\partial x_j}\left[v\left(\frac{\partial\bar{u}_i}{\partial x_j} + \frac{\partial\bar{u}_j}{\partial x_i}\right)\right] \tag{2.8}$$

Unlike N-S equations for laminar flow, there is a new term $\left(\overline{u_i'u_j'}\right)$ called the inertial turbulence tensor in turbulent flow. It can be written with the viscous term and called

as stress tensor which is given in equation 2.9. The stress tensor is composed of Newtonian viscous stress and turbulent stress tensor terms.

$$\tau_{ij} = v\left(\frac{\partial \bar{u}_i}{\partial x_j} + \frac{\partial \bar{u}_j}{\partial x_i}\right) - \left(\overline{u_\iota' u_j'}\right) \tag{2.9}$$

Since the stress tensor contains detailed information about the turbulence structure, creating a mathematical model is quite difficult. In this context, various turbulence models have been proposed in literature so far.

2.2 Turbulence Models

Most of turbulence models use eddy viscosity to determine the Reynolds stress as follows:

$$-\left(\overline{u_\iota' u_j'}\right) = v_t\left(\frac{\partial \bar{u}_i}{\partial x_j} + \frac{\partial \bar{u}_j}{\partial x_i}\right) - \frac{2}{3}\delta_{ij}K.E \tag{2.10}$$

where v_t is eddy viscosity, δ_{ij} is Kronecker's delta and K.E is turbulent kinetic energy which can be obtained by $\left(\overline{u_\iota' u_\iota'}\right)\big/2$. It should be noted that eddy viscosity is not a fluid property, it only depends on the state of turbulence. According to eddy viscosity approach made by Prandtl, it should alter according to distance from wall in a flow which are bounded with a wall. Thus, '*mixing length model*' has been proposed and eddy viscosity can be obtained in terms of mixing length as given in equation 2.11.

$$v_t = \left|\frac{\partial u}{\partial y}\right| - l_m^2 \tag{2.11}$$

Although this approach provides reasonable results for wall-bounded flows (without seperation), more general and more modern approaches for turbulence models has been developed up to the present. For instance, the eddy viscosity approach for LES applications was made by Joseph Smagorinsky [24] as given in equation 2.12.

$$v_t = \Delta x \Delta y \sqrt{\left(\frac{\partial u}{\partial x}\right)^2 + \left(\frac{\partial v}{\partial y}\right)^2 + \frac{1}{2}\left(\frac{\partial u}{\partial y} + \frac{\partial v}{\partial x}\right)^2} \tag{2.12}$$

The most commonly used turbulence models in practical engineering applications are briefly described below.

2.2.1 Spalart-Allmaras model

Spalarat Allmaras (SA) is a one-equation model that solves the transport equation for kinematic eddy turbulent viscosity. Generally, it provides acceptable results for wall-bounded aviation applications and it does not require finer grid resolution. It solves transport equation without calculating a length scale for eddy viscosity. The equation of this turbulence model is given in equation 2.13.

$$
\frac{\partial \tilde{v}}{\partial t} + u_j \frac{\partial \bar{v}}{\partial x_j} = C_{b1}[1 - f_{t2}]\tilde{S}\tilde{v} + \frac{1}{\sigma}\{\nabla * [(v + \tilde{v})\nabla\tilde{v}] + C_{b2}|\nabla\tilde{v}|^2\}
$$
$$
- \left[C_{w1}f_w - \frac{C_{b1}}{\kappa^2}f_{t2}\right]\left(\frac{\tilde{v}}{d}\right)^2 + f_{t1}\Delta U^2
$$
(2.13)

The right hand side (RHS) terms of the equation 2.13 represent the production, diffusion and destruction terms, respectively. Detailed information about these terms can be found in [29] and [30].

2.2.2 K-epsilon model

K-epsilon $(k - \varepsilon)$ model is the most commonly used turbulence model in CFD applications. In this model, turbulence modeling is performed using two transport equations. The purpose of this model is to develop the 'mixed length' model and apply it in more complex flows. The general transport equations in this model are suggested by Jones and Launder [31]. However the coefficients were proposed by Launder and Shartma [32]. The first variable "k" represents the energy in turbulence, whereas "ε" indicates the scale of turbulence. These two equations which model the turbulence phenomena are given in equation 2.14 and 2.15. First one is turbulence kinetic energy and the second one is the dissipation.

$$
\frac{\partial(\rho k)}{\partial t} + \frac{\partial(\rho k u_i)}{\partial x_i} = \frac{\partial}{\partial x_j}\left[\left(\mu + \frac{\mu_t}{\sigma_k}\right)\frac{\partial k}{\partial x_j}\right] + P_k + P_b + \rho\varepsilon - Y_M + S_k
$$
(2.14)

$$
\frac{\partial(\rho\varepsilon)}{\partial t} + \frac{\partial(\rho\varepsilon u_i)}{\partial x_i} = \frac{\partial}{\partial x_j}\left[\left(\mu + \frac{\mu_t}{\sigma_k}\right)\frac{\partial\varepsilon}{\partial x_j}\right] + \frac{C_{1\varepsilon}\varepsilon}{k}(P_k + C_{3\varepsilon}P_b) - \frac{C_{2b}\rho\varepsilon^2}{k} + S_\varepsilon
$$
(2.15)

2.2.3 K-omega model

K-Omega ($k - \omega$) is a turbulence model consisting of two equations. It includes two variables and k indicates the kinetic energy of the turbulence, while ω refers to the distribution of kinetic energy to the internal thermal energy. More information about this turbulence model can be obtained from [33].

$$\frac{\partial k}{\partial t} + U_j \frac{\partial k}{\partial x_j} = P_k - \beta * k\omega + \frac{\partial}{\partial x_j}\left[(v + \sigma_k v_T)\right]\frac{\partial k}{\partial x_j} \tag{2.16}$$

$$\frac{\partial \omega}{\partial t} + U_j \frac{\partial \omega}{\partial x_j} = \alpha S^2 - \beta \omega^2 + \frac{\partial}{\partial x_j}\left[(v + \sigma_\omega v_T)\right]\frac{\partial \omega}{\partial x_j} + \frac{2(1 - F_1)\sigma_{\omega 2}}{\omega}\frac{\partial k}{\partial x_i}\frac{\partial \omega}{\partial x_i} \tag{2.17}$$

In general, before selecting a turbulence model for any flow analysis, the attributes described below may provide a guidance [28].

- SA model will be excellent choice for the problems which boundary layers are attached and seperation existed such as flow around wing, fuselage or any type of external flow applications in aerospace. However, this model is not suitable for the complex circulations or convection applications such as heat transfer problems.

- Using ($k - \varepsilon$) model, a sensible selection can be done between robustness, computational cost and accuracy. It is mostly used in industry for the complex circulation problems. Unlike SA, this model can be applied to heat transfer problems.

- The last turbulence model ($k - \omega$) defined is basically similar with ($k - \varepsilon$) model. However, only the second turbulence variables are different. Its performance is also similar with ($k - \varepsilon$). It is also used in the field of aerospace. Thus, it can be an alternative model for SA.

- In Star-CCM+, there are several types of these turbulence models with some modifications. The most accurate choice for the turbulence model can be made using the information in software's user manual according to y+ value.

3. NUMERICAL IMPLEMENTATION

In this thesis, the aerodynamic efficiency of non-planar wing (C-wing) was examined. The experimental study of C-wing was carried out at Glasgow University, Aerospace Engineering Department by Shaun N. Skinner [5] as his PhD thesis under Dr. Hossein Zare-Betash supervision in June 2018. Numerical results obtained were validated with experimental data. General information about C-wing geometry is given in the next subsection.

3.1 Modeling of Geometry

The planar and non-planar wing configurations are shown in Figure 3.1 and Figure 3.2. As seen in Figure 3.2, C-wing configuration is basically composed of three parts which are top-wing, side-wing and main wing. The wing tip is curvatured like letter "C" in non-planar wing type in order to reduce the tip vortices occured.
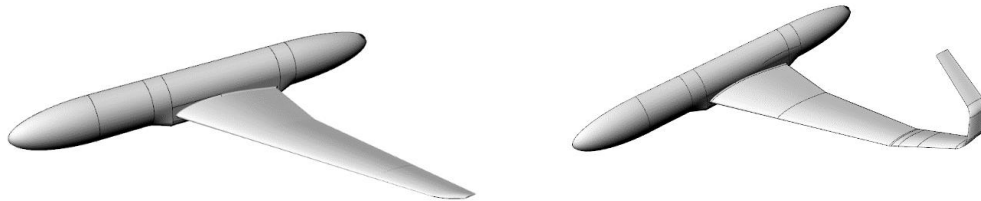
Figure 3.1. Planar and non-planar wing systems.
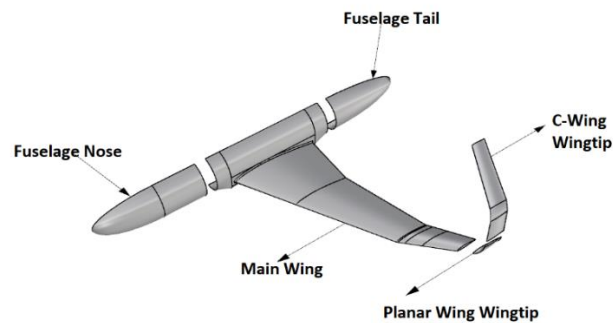
Figure 3.2. Main parts of C-wing configuration.

Since there is a symmetrical flow around aircraft, half body was modeled in numerical simulation as shown Figure 3.3
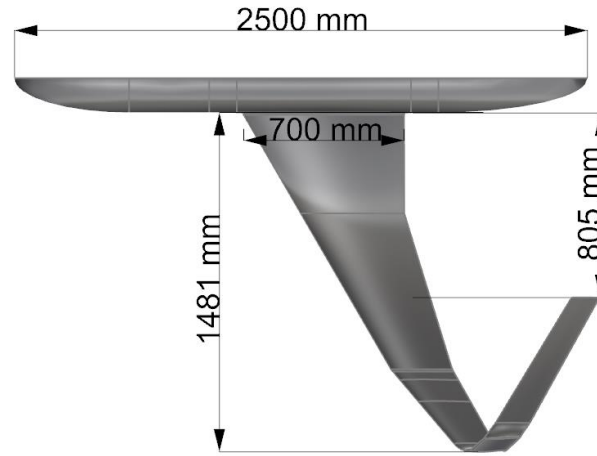
Figure 3.3. Main dimensions of half body of aircraft.

3.2 Computational Domain and Boundary Conditions

Since the Eulerian type approach is used in this study, a control volume and boundary conditions must be defined before solution. The diameter of control volume was selected four times the length of fuselage as shown in Figure 3.4.. Boundary conditions implemented for the control domain are given as,

- The boundary condition for farfield, is given as velocity inlet.

- The boundary condition for symmetry plane is given as symmetry.

- The boundary condition for body, is given as wall.
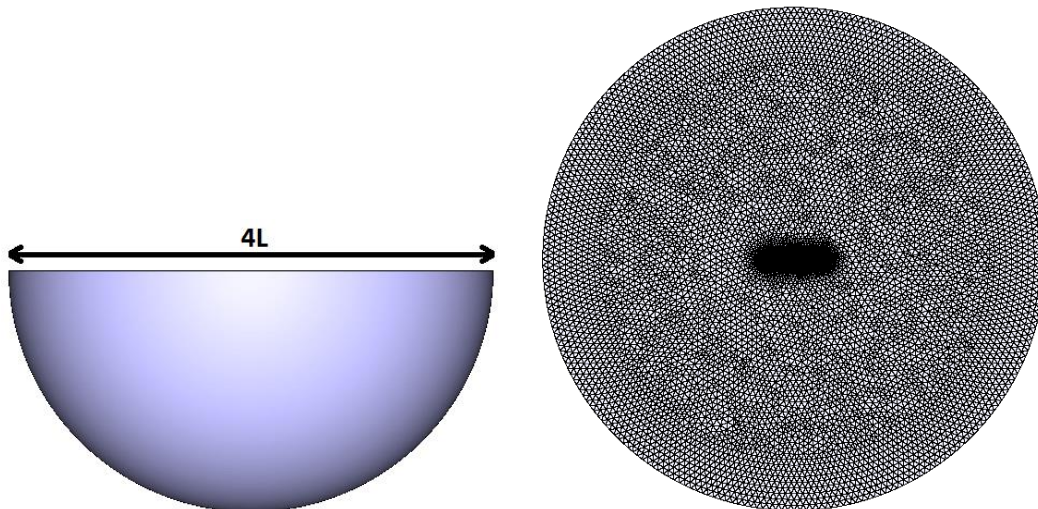
Figure 3.4. Semi spherical flow domain with farfield (left) symmetry (right) plane.

3.3 Mesh Generation

In this study, Pointwise [26] was used for generation of both surface and volume mesh. The mesh quality has been improved in sensitive areas such as the boundary layer, wing tip and wing vicinity to capture flow fields accurately. In Figure 3.5, the growth of grid elements can be seen around the whole geometry and it is obvious that grid size is getting coarser in the farfield. Since capturing flow seperations are quite important to get accurate results around the wing, mesh quality of the leading and trailing edges of wing must be higher. Therefore, quad mesh elements were generated in these regions. As the mesh gets away from the boundary layer, unstructured mesh is generated.
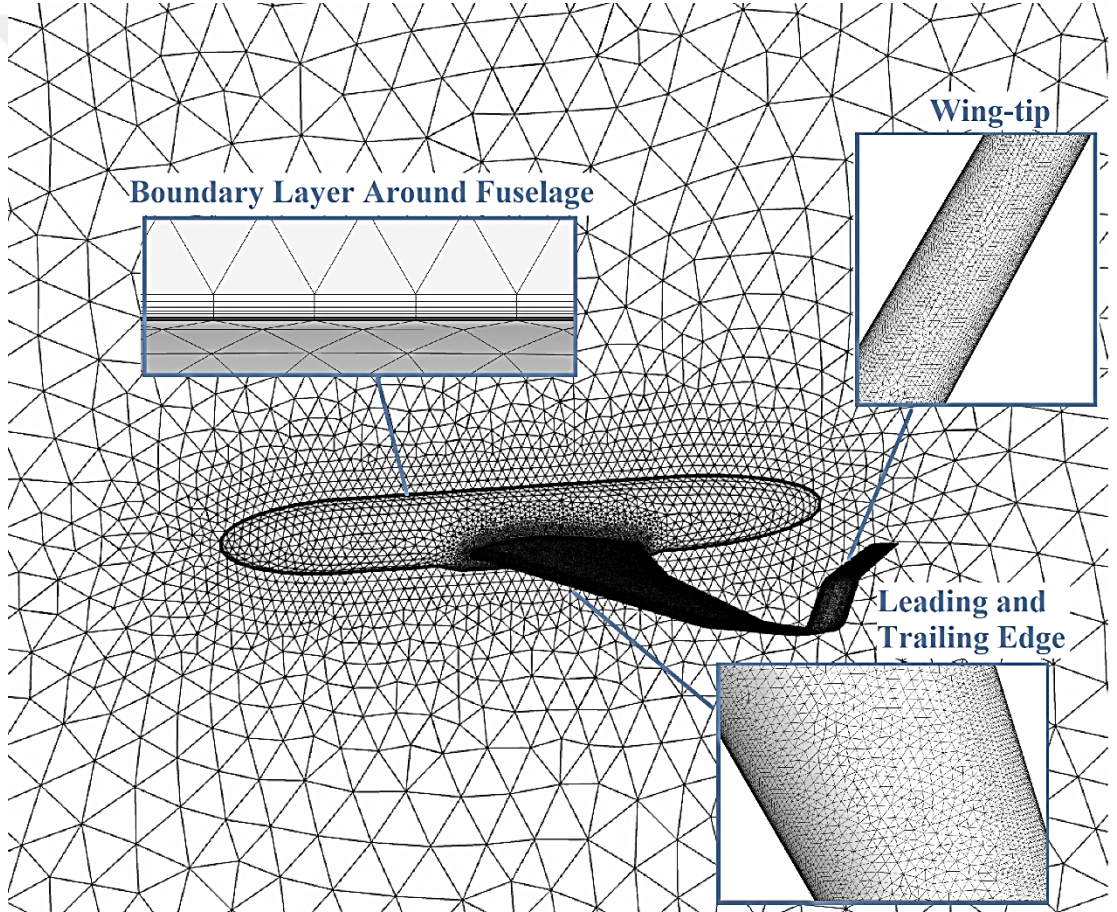
Figure 3.5. Surface and volume mesh distribution in computational domain.

The distance of first cell in boundary layer can be calculated using the expression given in equation 3.1.

$$y^+ = \frac{u^* y}{\vartheta} \tag{3.1}$$

Here, the frictional velocity is represented as u^* and distance of nearest cell to the wall is shown with y. In equation 3.2, frictional velocity equation is given.

$$u^* = \sqrt{\frac{\tau_w}{\rho}} \tag{3.2}$$

Total thickness of boundary layer is calculated using Prandtl's boundary layer formula for turbulent flows, which is given in equation 3.3. In this study, the boundary layer thickness around wing can be seen in Figure 3.6.

$$\delta_{BL} = \frac{0.16\,x}{Re_x^{1/7}} \tag{3.3}$$

Growth rate between prism layers and total number of layer was determined according to first layer thickness and total thickness of the boundary layer. Detailed information about the boundary layer thickness is given in the Table 3.1.

Table 3.1. Boundary layer parameters for wing and fuselage.

First Layer Thickness	0.007
Growth Rate	1.4
Number of Layer	19
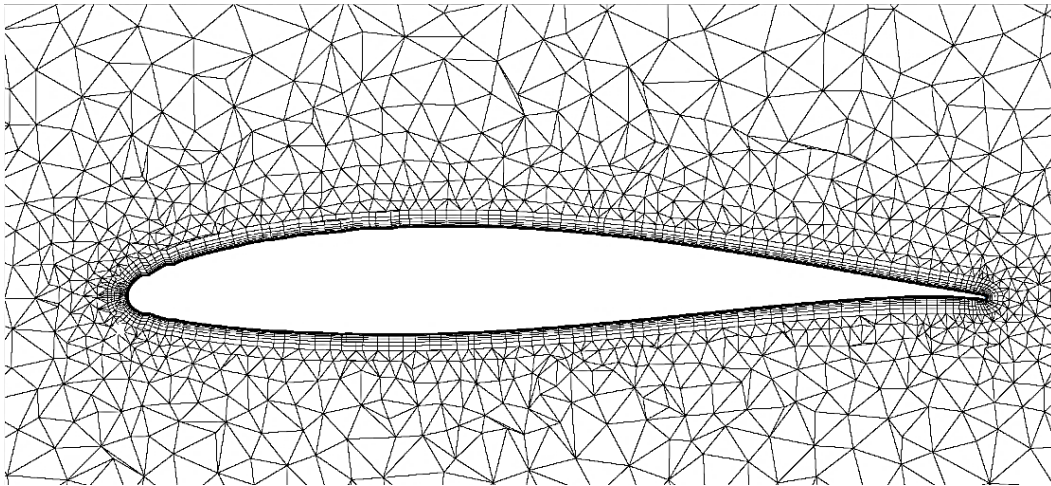
Figure 3.6. Boundary layer development around the wing.

After all refinements were performed, total number of mesh and type of the mesh elements were obtained as given in Table 3.2.

Table 3.2. Flow properties in the RANS simulations performed.

Surface Mesh		Volume Mesh			Total Domain
Quad	**Triangles**	**Tetrahedral**	**Pyramids**	**Prisms**	**Total Cell**
2318	124600	2522986	2608	1599076	4124670

3.4 Flow Conditions and Physical Model

After grid generation is completed physical model for flow solver was set up. For numerical simulations, a RANS based CFD solver Star-CCM+[28] was used. The setup parameters of the physical model can be seen in Table 3.3. The experimental conditions were used for the numerical simulations as given in Table 3.4.

Table 3.3. Physical model parameters used in Star-CCM+.

Flow property	Implicit Unsteady
Material property	Constant Air
Flow model	Segregated Flow
Viscous regime	Turbulent Flow
Turbulence model	$SST\ k - \omega$
Time step size	0.02

Table 3.4. Flow properties in the RANS simulations performed.

Parameters	**Units**	**Value**
Mach Number	-	0.41
Altitude	m	0
Dynamic Pressure	Pa	1532.25
Angle of Attack	deg	0,2,4,6,8,10,12

The RANS (Reynolds Averaged Navier-Stokes) equations were solved to calculate the velocity and pressure in computational domain. As Mach number is sufficiently low (<0.30), assumption of incompressibility can be considered in the simulations. Since flow seperations can not be neglected especially in higher angle of attacks (AoA), unsteady simulations were also performed. Since y+ value was set to be lower than one, the $SST\ k - \omega$ turbulence model was used to include turbulence effects into the problem.

4. OPTIMIZATION

4.1 Optimization Framework

In order to establish the optimization framework, it is necessary to select proper optimization variables and criteria applicable to a parametric model. In this study, Latin Hypercube sampling method which will be explained was used for choosing optimization parameters. Desired number of samples have been entered to the algorithm to generate cases randomly.

It is also desired to see the results of the intermediate points other than the number of samples entered. Since performing CFD analyses for every single point will be computationally expensive, a surrogate model was created by using the results obtained in sampling simulations. The high fidelity model of the optimization variables during the iterations created and used as a surrogate model. Kriging method is used to generate the model. Theoretical examination of Kriging method can be found in next subsections.

Optimum points of this response surface were obtained by using an optimization method and then final design was achieved. Conjugate Gradient method was used as a first order optimization method and for a second order method Quasi-Newton (Broyden–Fletcher–Goldfarb–Shanno and Finite Difference) procedure was used in this study.

4.1.1 Latin hypercube sampling method

In order to generate sampling with chosen optimization parameters, Latin Hypercube Method can be used. It is based on statistical definitions to make sampling. Range of each uncertainty variables in this technique can be broken into N_s segments of equal probability, where N_s represents the number of samples needed for the study. Each variable is selected randomly but has an equal probability segments. [21]

The most important advantage of sampling-based methods is that their applications are simple and they can work independently from relevant scientific disciplines in

analysis. On the other hand, disadvantage of this method is that a large number of functions must be calculated to obtain a converged statistical distribution. Therefore, it is computationally expensive. However, it still requires less sampling number than Monte Carlo method which uses a similar technique. It should be noted that LHS (Latin Hypercube Sampling) estimates the mean value more accurately than the random sampling.

4.1.2 Kriging method

In order to obtain results for any type of problem, it is essential to carry out experiments or numerical simulations for the engineering designs. These simulations can take long time depending on the problem of interest. For instance, when a flow around a wing is to be examined, it will take longer time as the fidelity level of the physical model increases. In addition, if an optimization study is to be added to this problem, it is necessary to repeat the analyzes for each iteration to optimize the selected set of parameters. This would be a computationally expensive effort. Instead, results can be obtained in a shorter time using a surrogate model during the optimization. Basically, this method can be defined as the modeling of response of simulator at a certain number of selected logical points. This method is also known as curve fitting if it is considered to be only a single variable.

In this thesis, Kriging method was selected as a surrogate model. Kriging method is a representative metamodeling technique originated from Geostatistics. The main goal is to create a representative model using the data for known points. These known points can be represented with $z(x_1)$, $z(x_2)$, .. $z(x_N)$ and the linear function we are looking for can be represented with $Z(x)$ where data point is denoted by x. In a control volume (V), these functions can be integrated as;

$$z_v = \frac{1}{V} \int_V z(x)\,dx \qquad (4.1)$$

In control volume, calculation of the Z(V) can be done taking weighted avarge of the data as;

$$z_{\dot{v}} = \sum \lambda_i z(x_i) \qquad (4.2)$$

$$Z_{\dot{v}} = \sum \lambda_i Z(x_i) \tag{4.3}$$

where λ_i denotes the weighting factors and $z_{\dot{v}}$ shows the weighted average. The following assumptions were made when these weights are selected.

- It is unbiased. This means $E[Z_{\dot{v}} - Z_v] = 0$.

- Variance is minimum. This means $Var[Z_{\dot{v}} - Z_v] = 0$.

The variable Z(x) is assumed to be stationary with mean value, m. Its mean at every point is equal to m. Mathematically it can be written as given in equation 4.4.

$$E[Z(x)] = m = E[Z_v] \tag{4.4}$$

The mean of error is $[Z_{\dot{v}} - Z_v]$ and can be written using equation 4.3 and 4.4 as given in equation 4.5.

$$E\left[\sum \lambda_i Z(x_i) - Z_v\right] = \sum \lambda_i m - m = m\left[\sum \lambda_i - 1\right] \tag{4.5}$$

Second assumption for the weights is about the minimization of variance. The variance of error can be written in terms of covariance as shown in equation 4.6.

$$\begin{aligned}
\sigma^2 &= \sum\sum \lambda_i\lambda_j C(x_i, x_j) + \bar{C}(V,V) - 2\sum \lambda_i \bar{C}(x_i, V) \\
&= 2\sum \lambda_i \bar{\gamma}(x_i, V) - \sum\sum \lambda_i\lambda_j \gamma(x_i, x_j) + \bar{\gamma}(V,V)
\end{aligned} \tag{4.6}$$

where $\bar{\gamma}(x_i, V)$ represents the average between x_i and V and it can be obtained using equation 4.7.

$$\bar{\gamma}(x_i, V) = -\frac{1}{V}\int_V \gamma(x_i - x)dx \tag{4.7}$$

$\bar{C}(x_i, V)$ and $\bar{C}(V,V)$ show the averages for the covariance. In order to minimize the estimation, variance under the constraint must be equal to 1. It can be shown using a Lagrange multiplier (μ) to minimize the estimation variance. Since the sum of the weights must be 1.0, Lagrange multiplier does not change the value of expression. The esssential step in deriving the kriging equations is minimizing the expression which is given in the equation 4.8.

$$\phi = 2\sum \lambda_i \bar{\gamma}(x_i, V) - \sum\sum \lambda_i\lambda_j\gamma(x_i, x_j) + \bar{\gamma}(V, V) + 2\mu\left(1 - \sum \lambda_i\right) \quad (4.8)$$

It can be done by taking derivative of the equation 4.8 with respect to each unknown and let them be equal to zero using the following two assumptions made:

- $\gamma_{ij} = \gamma(x_i, x_j)$

- $\gamma_{iV} = \bar{\gamma}(x_i, V)$

$$\phi = 2\lambda_1\bar{\gamma}_{1V} + 2\lambda_2\bar{\gamma}_{2V} + 2\lambda_3\bar{\gamma}_{3V}$$
$$- (\lambda_1^2\gamma_{11} + \lambda_2^2\gamma_{22} + \lambda_3^2\gamma_{33} + 2\lambda_1\lambda_2\gamma_{12} + 2\lambda_1\lambda_3\gamma_{13} \quad (4.9)$$
$$+ +2\lambda_2\lambda_3\gamma_{23}) - \bar{\gamma}(V, V) + 2\mu(1 - \lambda_1 - \lambda_2 - \lambda_3)$$

After taking derivative of the equation 4.9 according to $\lambda_1, \lambda_2, \lambda_3, \mu$ and let theem be equal to zero, following equations were obtained.

$$\lambda_1\gamma_{11} + \lambda_2\gamma_{12} + \lambda_3\gamma_{13} + \mu = \bar{\gamma}_{1V} \quad (4.10)$$

$$\lambda_1\gamma_{12} + \lambda_2\gamma_{22} + \lambda_3\gamma_{23} + \mu = \bar{\gamma}_{2V} \quad (4.11)$$

$$\lambda_1\gamma_{13} + \lambda_2\gamma_{23} + \lambda_3\gamma_{33} + \mu = \bar{\gamma}_{3V} \quad (4.12)$$

$$\lambda_1 + \lambda_2 + \lambda_3 = 1 \quad (4.13)$$

The equations 4.10, 4.11, 4.12, 4.13 can be defined with two equations using Einstein summation and it will look like as in equations 4.14 and 4.15.

$$\sum_{j=1}^{3} \lambda_j\gamma(x_i, x_j) + \mu = \bar{\gamma}(x_i, V) \qquad i = 1,2,3 \quad (4.14)$$

$$\sum_{i=1}^{3} \lambda_i = 1 \quad (4.15)$$

In order to solve this system, it can be written as matrix form as follows. $[A][x] = [B]$

$$\begin{bmatrix} \gamma_{11} & \gamma_{12} & \gamma_{13} & \cdots & \gamma_{1N} & 1 \\ \gamma_{21} & \gamma_{22} & \gamma_{23} & \cdots & \gamma_{2N} & 1 \\ \vdots & \vdots & \vdots & \vdots & \vdots & \vdots \\ \gamma_{N1} & \gamma_{N2} & \gamma_{N3} & \cdots & \gamma_{NN} & 1 \\ 1 & 1 & 1 & \cdots & 1 & 0 \end{bmatrix} \begin{bmatrix} \lambda_1 \\ \lambda_2 \\ \vdots \\ \lambda_N \\ \mu \end{bmatrix} = \begin{bmatrix} \bar{\gamma}(x_1, V) \\ \bar{\gamma}(x_2, V) \\ \vdots \\ \bar{\gamma}(x_N, V) \\ 1 \end{bmatrix} \quad (4.16)$$

If γ value is acceptable, then matrix A is always non-singular. This means that a solution exists and it is unique. Furthermore, Kriging variance is given in equation 4.17 using the expressions obtained from equation 4.6 and 4.16.

$$\sigma_K{}^2 = x^T B - \bar{\gamma}(V, V) \quad (4.17)$$

Kriging method creates a surrogate model using the results obtained from numerical simulations, thus lower fidelity results can be obtained using the Kriging model instead of running high fidelity analyses for each iteration. In this study, the surrogate model was created using the numerical results obtained from analyzes with random variables selected by LHS.

4.1.3 First order optimization method

After surrogate model and response surface were created, an optimization method must be carried out to find the best scenario with maximum aerodynamic efficiency. As a first order method, CGM (Conjugate Gradient Method) was employed. CGM is an iterative method which solves particular systems of linear equations numerically. It can be used for either numerical solution of PDEs or optimization problems. Actually, this method is a modification of SDM (Steepest-Descent Method) so that it is very simple to implement. CGM is guaranteed to converge to a local minimum point of a function. Directions of the gradients are not orthogonal to each other, whereas they are orthogonal with respect to matrix A which is symmetric and is positive definite. It can be shown mathematically as;

$$\vec{d}^{(i)T} A \, \vec{d}^{(j)} = 0 \qquad \text{for all i and j} \qquad i \neq j \quad (4.17)$$

The algorithm of CGM is expressed below and it should be noted that the first step of CGM is the same with SDM.

- **Step 1**

First step starts with estimating inital design (x^0). Iteration counter (k) must be zero and stopping criteria (ε) must be set. After all these are specified, direction of the first step can be calculated using equation 4.18.

$$\vec{d}^{(0)} = -\vec{c}^{(0)} = -\nabla f(x^{(0)}) \tag{4.18}$$

After the first direction was determined, stopping criteria must be checked. If the condition of $||\vec{c}^{(0)}|| < \varepsilon$ is satisfied, then iterations must be stopped.

- **Step 2**

Gradient of the cost function must be calculated in this step as given in equation 4.19.

$$\vec{c}^{(k)} = \nabla f(x^{(k)}) \tag{4.19}$$

If the condition of $||\vec{c}^{(k)}|| < \varepsilon$ is satisfied, then iterations must be stopped.

- **Step 3**

In the third step, direction of the new conjugate must be calculated as;

$$\vec{d}^{(k)} = -c^{(k)} + \beta_k\, d^{(k-1)} \tag{4.20}$$

where β_k is:

$$\beta_k = \left(\frac{||\vec{c}^{(k)}||}{||\vec{c}^{(k-1)}||}\right)^2 \tag{4.21}$$

- **Step 4**

In step four, the step size α_k which minimize the $f\left(\vec{x}^{(k)} + \alpha_k \vec{d}^{(k)}\right)$ must be calculated. In this thesis to minimize that function line search method was used in Dakota [22].

- **Step 5**

New design must be updated in the fifth step and then go back to step 2.

$$\vec{x}^{(k+1)} = x^{(k)} + \alpha_k\, d^{(k)} \tag{4.22}$$

At the end descent condition, $\vec{c}^{(k)} * d^{(k)} < 0$ must be checked. Instead of $d^{(k)}$, equation 4.20 can be written and descent condition for CGM will be as the following.

$$\vec{c}^{(k)}\left[-c^{(k)} + \beta_k \, d^{(k-1)}\right] = -\left|\left|\vec{c}^{(k)}\right|\right|^2 + \vec{c}^{(k)} \left(\frac{||\vec{c}^{(k)}||}{||\vec{c}^{(k-1)}||}\right)^2 d^{(k-1)} \tag{4.23}$$

Right hand side of Equation 4.23 will be negative if the second term is zero. Then its condition for CGM will be as given in equation 4.24.

$$\vec{c}^{(k)} d^{(k-1)} = 0 \tag{4.24}$$

4.1.4 Second order optimization methods

As a second order optimization method Quasi-Newton (QN) method was performed. In this method, a solution is proposed to update inverse of the Hessian matrix in each iteration. There are several approaches to update it. In this thesis, Brodyen Fletcher-Goldfarb-Shanno (BFGS) and Finite Difference Methods (FDM) was used. In the below, the steps of the Quasi Newton algorithm and determination of the Hessian matrix was given.

- **Step 1**

Firstly initial design $x^{(0)}$ should be calculated. Then, initial Hessian matrix $H^{(0)}$ should be estimated. In this method, it is assumed that $H^{(0)} = I$. Also a convergence parameter (ε) must be selected to finish optimization procedure. For the initial step $(k = 0)$ gradient vector can be obtained as:

$$\vec{c}^{(0)} = \vec{\nabla} f(x^{(0)}) \tag{4.25}$$

- **Step 2**

The value of the norm of the gradient vector must be checked. If it is less than the convergence criteria, iterative process must be ended. Otherwise it should be continued.

$$\left|\left|\vec{c}^{(0)}\right|\right| < \varepsilon \tag{4.26}$$

- **Step 3**

To obtain the search direction $(d^{(k)})$, the following linear system of equations should be solved.

$$H^{(k)}d^{(k)} = -c^{(k)} \qquad (4.27)$$

- **Step 4**

The step size (α_K) must be calculated which minimizes $f(x^{(k)} + \alpha d^{(k)})$. In this thesis to minimize that function, the line search method was used in Dakota [22].

- **Step 5**

After the step size is obtained, the design change is used to update the design as in equation 4.28.

$$\vec{x}^{(k+1)} = x^{(k)} + \alpha_k \, d^{(k)} \qquad (4.28)$$

- **Step 6**

According to the BFGS method, Hessian approximation is done as given in below.

$$H^{(k+1)} = H^{(k)} + D^{(k)} + E^{(k)} \qquad (4.29)$$

where $D^{(k)}$ and $E^{(k)}$ are,

$$D^{(k)} = \frac{y^{(k)}y^{(k)^T}}{(y^{(k)}.\ s^{(k)})}$$

$$\qquad (4.30)$$

$$E^{(k)} = \frac{c^{(k)}c^{(k)^T}}{(c^{(k)}.\ d^{(k)})}$$

In equation 4.30 $s^{(k)}, y^{(k)}, c^{(k+1)}$ represent the change in design, the change in gradient and the gradient vector, respectively.

$$s^{(k)} = \alpha_k \, d^{(k)}$$

$$y^{(k)} = c^{(k+1)} - c^{(k)} \qquad (4.31)$$

$$c^{(k+1)} = \nabla f(x^{(k+1)})$$

As an alternative approach, the Dakota software [22] uses the finite difference method (FDM) for calculation of the Hessians in optimization process. Generally, a first-order forward difference of gradients is used to estimate the ith Hessian column when gradients are analytically available as given below.

$$\nabla^2 g_i(k) \cong \frac{\nabla g_i(x+he_i) - \nabla g_i(x)}{h} \qquad (4.32)$$

When the gradients are not directly avaliable then the second-order approximation can be done as given in equation 4.33.

$$\nabla^2 g(k) \cong \frac{g(x+he_i+he_j) - g(x+he_i-he_j) - g(x-he_i+he_j) + g(x-he_i-he_j)}{4h^2} \qquad (4.33)$$

- **Step 7**

After the Hessian matrix is obtained, we set $k = k + 1$ and turn to the step 2.

4.2 CFD Based Optimization

As mentioned above, analyses and optimization tools to be used here must be coupled with each other as shown in Figure 4.1. First a representative parametric model should be created in the loop, then this model is exported to the grid generation program to discretize the body and computational domain. Subsequently, this discretized domain is transferred to flow solver and simulation is performed until convergence is achieved. Detailed information about these tools are given in the following subsections.
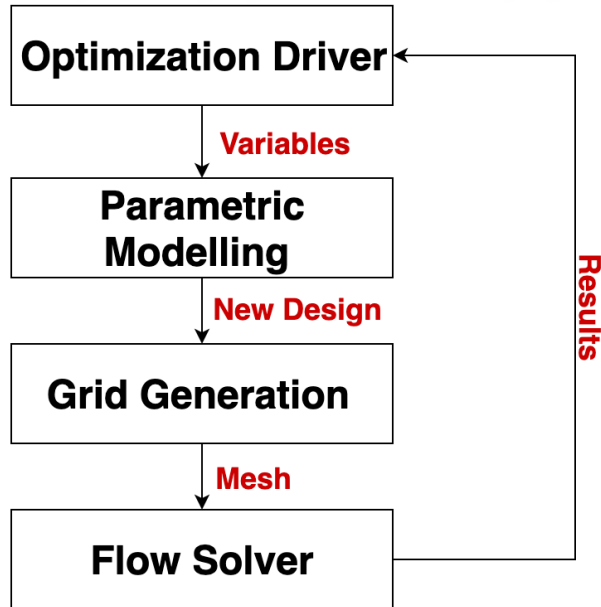
Figure 4.1. Workflow diagram of the CFD based optimization study.

4.2.1 Parametrical modelling

The first step in optimization applications is creating a parametric model. The optimization process is not carried out manually, but in coordination with multiple

tools. Changes in geometry for each scenario require generation of new mesh, thus extra drivers are needed. In order to recognize these changes in geometry, CAD models should be made parametrically. Thus, new geometries will be updated automatically for each new variable set defined.

In this thesis, the geometry for each scenario was created using OpenVSP which is an open source CAD tool provided by NASA [27]. In addition, a script was written to create the new geometry automatically using C/C++ language. Since it is not possible to import the original geometry in OpenVSP, the representative model was generated by using the the pictures of original geometry in the background in OpenVSP.

4.2.2 Automatic grid generation

The geometry is updated for each iteration with the changes made in the optimization variables. Mesh elements also need to be updated as the variables of geometry are updated in every simulation. Therefore, an algorithm is needed to create mesh elements automatically.

In this thesis, Pointwise was used for grid generation procedure. The aircraft mesher (AM) is a pre-prepared script which was developed by Travis Carrigan [23]. AM can be run with Pointwise and all grid generations in this study were carried out using this script. Briefly, it generates both surface and volume meshes around anaircraft using triangular and quad elements. After inserting the required parameters such as BL thickness, number of layers, etc. as inputs, it creates a discretized hemispherical control volume for numerical simulations.

In order to perform meshing process accurately, some supplementary codes were developed so that the geometry is to be imported from OpenVSP. Since the geometry is imported as surface, it should be named according to surface name identified in the mesh generation tool. In AM for this study, there are total of six database groups which are specified as fuselage, fairing, wing-upper, wing-lower, wing-tip, wing-trailing-edge. Name of the imported geometry was renamed and merged according to these mentioned names.

After these steps are achieved, the mesh generated must be exported to the flow solver (Star-CCM+) and boundary conditions must be implemented automatically in each analysis. Similarly, some additional codes were developed for these coupling and updating processes.

4.2.3 Optimization tool

The optimization tool works as a driver in the general computational framework. Applying the variable values given under certain constraints for the geometry, it generates new designs, perform the flow simulations and checks the optimality conditions for the updated designs. The optimization driver enables the coupled work scheme for parametric modeling, grid-generation and flow analysis.

Dakota which has been developed by Sandia National Laboratories [22] was used in this thesis for the optimization scheme . Kriging method was selected to create the surrogate model and Dakota selects random values in each case for three different parameters of C-wing using LHS algorithm and send them into the parametrical modelling tool. After a loop was completed, Dakota saves the results and starts new case. Using all of the results obtained, surrogate model was created and Dakota found the optimum geometry using the surrogate model in terms of aerodynamic efficiency (C_L/C_D).

4.2.4 Flow solver

A physical model was created in the flow solver for each case of modified geometry. Incompressible RANS based CFD solver (Star-CCM+) was used to obtain pressure and velocity fields. Results were saved at the end of each case in order to determine the optimum point in terms of drag and lift coefficients. A script was written to create the physical model for imported mesh from AM. Results obtained were exported as a *.csv file which are read by Dakota in each case. Details of the physical model were explained in Section 3.4.

5. VERIFICATION and VALIDATION

The reliability of numerical results should be examined in order to understand the accuracy of a computer-based study. There are some applications and some procedures which are known as Verification and Validation (V&V) studies. The verification process is addressing the quality of the numerical treatment of the model used in prediction, and the validation process defines the quality of numerical model. V&V is essential for numerical studies, and several works exist in literature about this topic. Studies of Roache [18] and Stern et al. [19] can be regarded as noteworthy works on this subject in engineering applications. Generally speaking, definition of V&V can be given with two fundamental questions as follows:

- Validation: Are we building the right system?

- Verification: Are we building the system right?

In CFD simulations, verification and validation (V&V) study is actually performed to understand the grid effects on numerical results. In this thesis, the methodology proposed by Stern et al. [19] for CFD simulations was followed. The grid convergence was investigated for the case of AoA=0 (deg) for the C-Wing configuration. The quantities were selected as lift (C_L) and drag coefficients (C_D). Since unstructured grid elements were used in this thesis, it is hard to estimate grid uncertainty. Hence, Richardson extrapolation method was utilized for the grid convergence with three mesh sizes. Refinement ratio was taken as $\sqrt{2}$ due to limited capacity of computational power.

According to Stern's procedure [19], initially the grid convergence ratio (R_G) must be calculated for verification. It is defined as;

$$R_G = \frac{\varepsilon_{G_{21}}}{\varepsilon_{G_{32}}} \tag{5.1}$$

where $\varepsilon_{G_{21}}$ and $\varepsilon_{G_{32}}$ are defined as difference between the results of medium (S_2) - fine (S_1) and coarse (S_3) - medium (S_2) meshes, respectively.

$$\varepsilon_{G_{21}} = S_2 - S_1 \tag{5.2}$$

$$\varepsilon_{G_{32}} = S_3 - S_2 \tag{5.3}$$

According to value of R_G, four different conditions can be possible:

- Monotonic Convergence

$$0 < R_G < 1$$

- Oscillatory Convergence

$$-1 < R_G < 0$$

- Monotonic Divergence

$$R_G > 1$$

- Oscillatory Divergence

$$R_G < -1$$

Grid uncertainty (U_G) and numerical error $(\delta^*_{RE_G})$ are defined using Richardson extrapolation technique and these terms can be calculated using the equation 5.4 and 5.5. In equation 5.4, S_U and S_L represent the lower and upper values of results.

$$U_G = |\frac{1}{2}(S_U - S_L)| \tag{5.4}$$

$$\delta^*_{RE_G} = \frac{\varepsilon_{G_{21}}}{r_G^{p_{G_{est}}} - 1} \tag{5.5}$$

where r_G denotes the refinement ratio in each direction (x,y,z) and it was taken as $\sqrt{2}$ to put a limitation for the total grid elements due to limited computational resource and $p_{G_{est}}$ represents the order of accuracy and can be calculated using equation 5.6.

$$p_{G_{est}} = \frac{\ln(\varepsilon_{G_{32}}/\varepsilon_{G_{21}})}{\ln(r_G)} \tag{5.6}$$

In order to make a correction in equation 5.5, a correction factor is defined as:

$$C_G = \frac{r_G^{p_G} - 1}{r_G^{p_{G_{est}}} - 1} \tag{5.7}$$

where theoretical order of accuracy is represented with p_G in equation 5.7 and it is generally taken as 2. If C_G is close to 1, it means how close the solutions are to the asymptotic range. In this case, numerical error (δ_{SN}^*), benchmark result (S_C) and the corrected grid uncertainty(U_{G_C}) are calculated as follows.

$$\delta_{SN}^* = C_G\, \delta_{RE_G}^* \tag{5.8}$$

$$S_C = S - \delta_{SN}^* \tag{5.9}$$

$$U_{G_C} = \begin{cases} (2.4(1 - C_G)^2 + 0.1)\left|\delta_{RE_G}^*\right| & |1 - C_G| < 0.125 \\ |1 - C_G|\left|\delta_{RE_G}^*\right| & |1 - C_G| \geq 0.125 \end{cases} \tag{5.10}$$

But in the second scenario, if C_G is sufficently less or greater than 1 that means solutions are not in the asymptotic range and grid uncertainty (U_G) can be calculated using equation 5.11.

$$U_G = \begin{cases} (9.6(1 - C_G)^2 + 1.1)\left|\delta_{RE_G}^*\right| & |1 - C_G| < 0.125 \\ (2|1 - C_G| + 1)\left|\delta_{RE_G}^*\right| & |1 - C_G| \geq 0.125 \end{cases} \tag{5.11}$$

Finally, validation uncertainty (U_V) can be calculated as:

$$U_V = \sqrt{U_G^2 + U_D^2} \tag{5.12}$$

where U_D is total experimental uncertainty.

Using the procedure provided by Stern et al. [19], a GUI (Graphical User Interface) was developed on MATLAB environment and a sample screenshot of the program is shown in Figure 5.1.

Figure 5.1. A sample screenshot of Verification and Validation programme.

User first should select the convergence type according to the results obtained in numerical simulation. Input section is required to be filled with numerical and experimental results, grid refinement ratio, lower and upper values of last two oscillation and experimental uncertainty value if available. After all parameters are inserted, outputs can be calculated by hitting the *RUN* button. As seen from Figure 5.1, output section is divided as verification and validation results. The uncertainty values of grid (U_G) and iteration (U_I) can be examined in the verification part, while relative error of numerical result (E) and validation uncertainty (U_V) are given as percentages in the validation part. According to selected grid refinement ratio r, total number of mesh elements and results of C_D and C_L are given in Table 5.1.

Table 5.1. Selected quantities and number of elements in V&Vstudy.

Quantities	Numer of Elements			EFD
	3.4M (S_3)	4.5M (S_2)	6.3M (S_1)	Data (D)
C_L	0.2317	0.2347	0.2338	0.2518
C_D	0.0256	0.0235	0.0234	0.0236

The V&V results obtained are given in Table 5.2. First, the grid refinement ratio must be calculated to determine convergence type whether it is monotonic or oscillatory. In this study, the results of C_D converged monotonically (R = 0.0416), whereas

convergence of C_L is found to be oscillatory (R = -0.3). Then the correction factor C_G was calculated as described above and the value of grid uncertainty U_I was determined. For instance, since calculated C_G for the drag force coefficient is sufficiently greater than 1, uncertainty values obtained can be used directly, thus no correction factor is required. It should be also noted that iterative uncertainty was neglected here as it was calculated sufficiently small compared to grid uncertainty. For the validation section, validation uncertainty and relative error were compared. If relative error E is found to be smaller than validation uncertainty U_V, this means that numerical results obtained are validated. The results of validation study are given in Table 5.2. Grid uncertainty values were calculated in a reasonable level such as 0.85 for drag coefficient and 0.64 for lift coefficient, and it shows that the impact of mesh size on the numerical results is sufficiently low. On the other hand, the numerical result of C_D is validated with the experimental data, while the result of C_L is not. The value of C_L was not validated because the relative error E was found to be higher than the validation uncertainty U_V.

**Table 5.2.** Verification and validation results for the quantities (C_D and C_L).

Condition	C_D Monotonic Convergence	C_L Oscillatory Convergence
$\varepsilon_{G_{21}}$	0.0001	0.0009
$\varepsilon_{G_{32}}$	0.0024	-0.0030
R_G	0.0416	-0.3000
p_{Gest}	9.1739	-
C_G	23.010	-
$U_G\%S_1$	0.8366	0.6415
$|E|\%D$	0.8474	9.4149
$U_V\%D$	2.1652	0.5817

6. RESULTS

6.1 Numerical Results of Planar and C-Wing Configurations

For the numerical simulations, StarCCM+ was used as an incompressible RANS based solver and results obtained were compared with experimental data [5] in terms of drag and lift coefficients. Each simulation in this study was performed using Intel(R) Xeon(R) CPU with 8 cores, clock speed 3.10 GHz and 16 GB of physical memory and each analysis converged approximately in 40 minutes using the current numerical model. Figure 6.1 shows the comparison of results of experiments for planar wing and C-wing configurations, with that of numerical results for various AoAs.
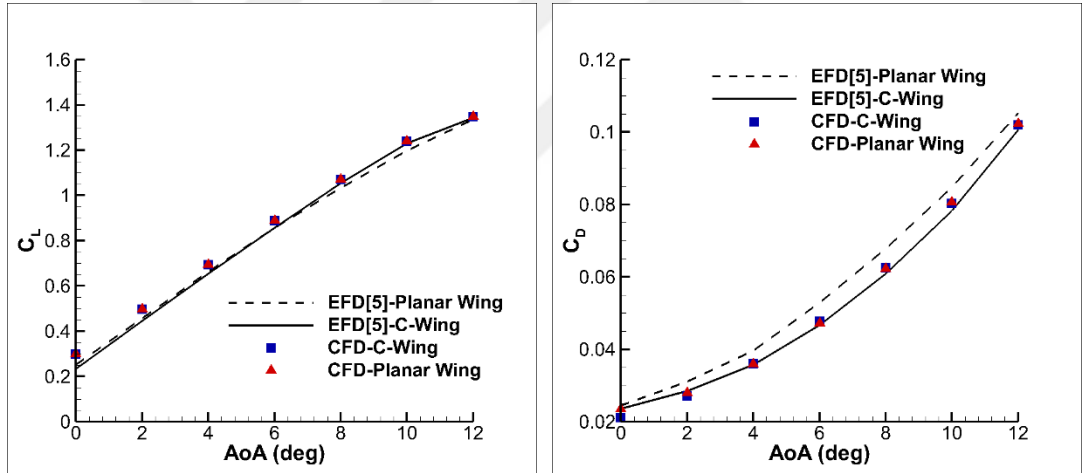

Figure 6.1. Lift (left) and drag (right) coefficients for different AoAs.

According to the results of experiment, it can be seen that the planar wing produces more drag force than that of C-wing configuration. This phenomena can be briefly explained by the reduction of tip vortices (induced drag) on C-wing design. In Figure 6.1, numerical results of C_D and C_L seem to be compatible with experimental data even for higher AoAs ($> 10°$). Average relative errors for C_D and C_L were calculated in a reasonable level of accuracy such as 8% and %6 for planar wing, while they are 1.5% and 3.0% for C-wing.

Figure 6.2 shows the comparison of aerodynamic efficiency (C_L/C_D) of C-wing configuration. Numerical results agree well with the experiments with an average

relative error of 2.4%. It can be also noted that difference between two configuration becomes clear between 2°<AoA<8°. This indicates the high aerodynamic efficiency of C-wing compared to traditional wing designs due to reduction of tip vortices occured at the tip of wings.
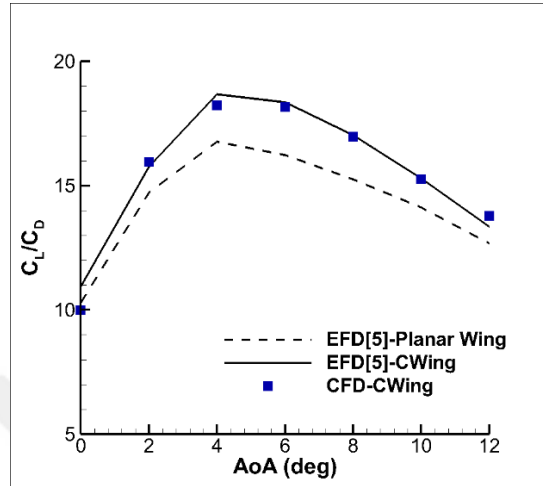
Figure 6.2. Comparison of experimental and numerical results for planar and C-wing configurations in terms of aerodynamic efficiency (C_L/C_D).

As widely known, induced drag is the drag component caused by the production of lift by the lifting surfaces, which can include the fuselage as well as the wings and tail. Parasitic drag is composed of form drag, skin friction drag, and interference drag. In this context, total drag force coefficient predicted in numerical simulations was divided into shear (parasitic drag) and pressure (induced drag) components and it was deduced that a considerable portion of the total drag force is composed of induced drag component.
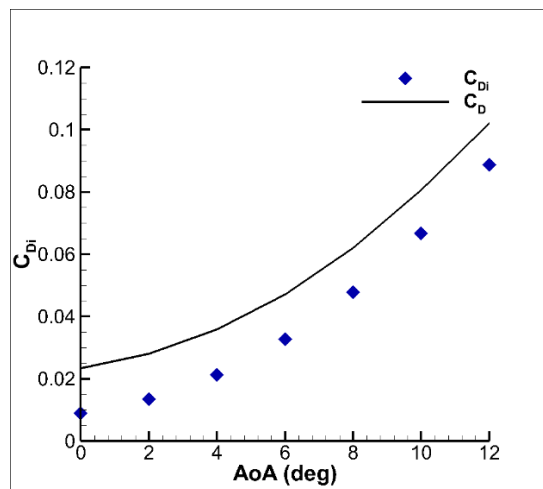
Figure 6.3. Results of total drag and induced drag coefficients of C-wing configuration with respect to AoAs.

40

Figure 6.3 shows the induced drag and total drag coefficients. Approximately, the induced drag component constitutes 40% of the total drag force for AoA=0. However, this ratio tends to increase up to 85% at AoA=12. It should be noted that this proportions of induced drag were obtained at one speed ($M = 0.41$), it may decrease as the speed of aircraft increases.

In Figure 6.4, y+ distribution on the body is given. Since usage of $k - \omega$ turbulence model requires y+< 1, the nearest cell to wall should be located according to this restriction. As seen Figure 6.4, all y+ values on the surface are less than one.
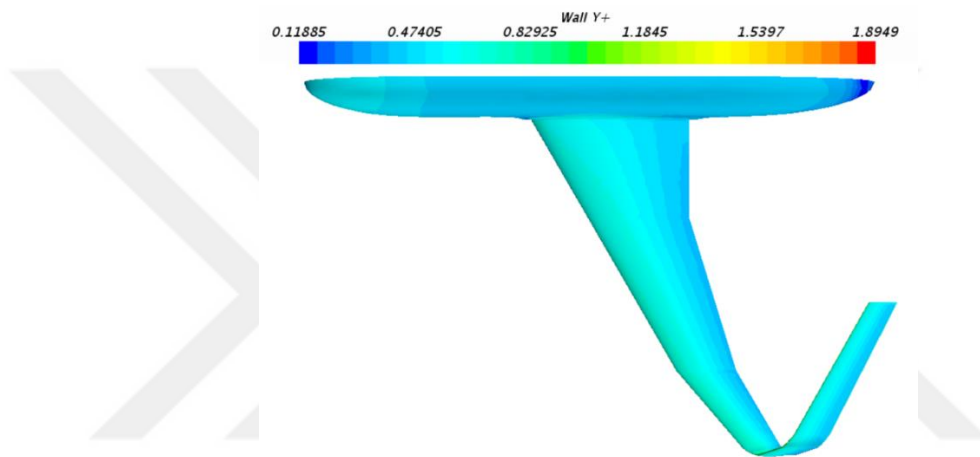

Figure 6.4. y+ distribution on the surface of aircraft at $M = 0.145$.

Since the aim of designing such a non-planar wing configuration (C-shaped) is to obtain a new geometry which has lower induced drag component, both planar and C-wing geometries were compared in terms of streamtraces. In Figure 6.5, the streamlines around wing was indicated on a selected slice. Contours on the slice show the velocity component in z-direction. Since the tip vortices will occur from bottom to top side of the wing, vertical velocity component was selected as a quantity. It should be also emphasised that, velocity gradient always occurs on the wing tip because of the pressure differences between lower and upper side of the wing and this difference will produce an extra drag force on the aircraft. However, using C-shaped wing configuration (see Figure 6.6), the effect of velocity gradient will be felt less on the wing compared to the planar wing (see Figure 6.5).
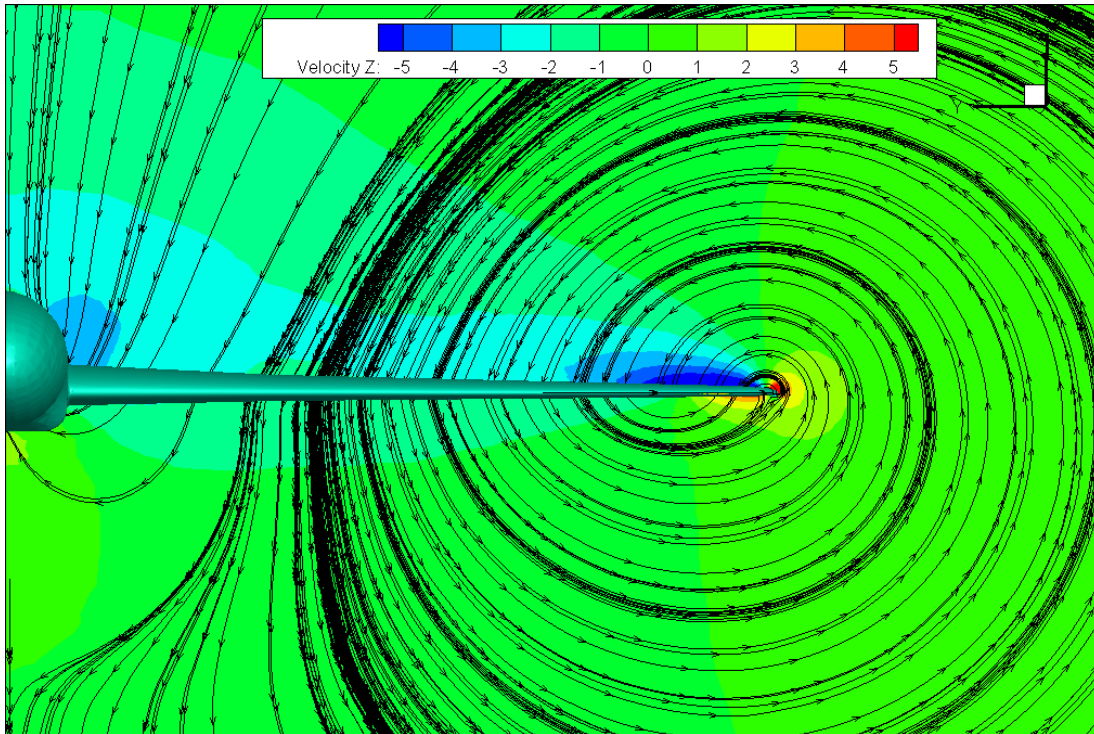
Figure 6.5. Streamtraces for the planar wing geometry at zero angle of attack.
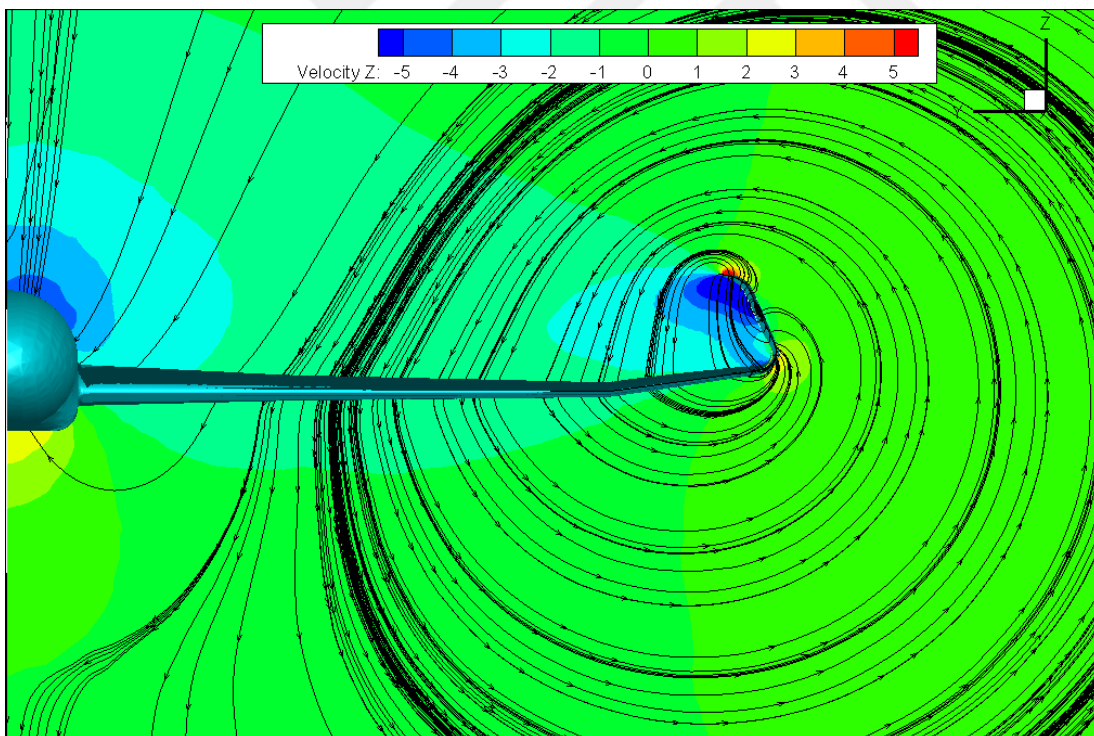

Figure 6.6. Streamtraces for the initial C-wing geometry at zero angle of attack.

6.2 Optimization Results for C-Wing Configuration

In this thesis, the optimization study was carried out for obtaining the optimum geometry which gives maximum aerodynamic efficiency (C_L/C_D). As it is explained in section 4.1, the optimization work starts with creating the parameteric model of the original geometry. Subsequently, the optimization variable value which have been transferred from Dakota were updated in the parametric model. These values were randomly determined by LHS (Latin Hypercube Sampling) method in Dakota for a certain number of cases. The computational grids were generated using AM (Aircraft Mesher) and it was exported to incompressible RANS solver (StarCCM+) in order to obtain numerical results. Kriging method was utilized to create the surrogate model and response surface. Finally, using CGM (Conjugate Gradient Method) and Quasi Newton Methods with two different Hessian approach, optimum geometry was obtained in terms of aerodynamic efficiency (C_L/C_D) under certain constraints.

OpenVSP was used for parametrical modelling in the first step of optimization. This tool does not allow to import any CAD geometry to the workspace, thus the original geometry has been approached with small shape errors that doesn't have significant effect on the results (C_L and C_D). This model is called as representative model for the optimization part and the results were compared with this model. The values of C_L and C_D of representative model was calculated as 0.1705 and 0.0220, respectively.

In Figure 6.7, three selected variables for the optimization proccess are shown. Using LHS method, this variables were shuffled and random scenarios were created. In this study, 25 samples were generated according to the variables which are given in Table 6.1.
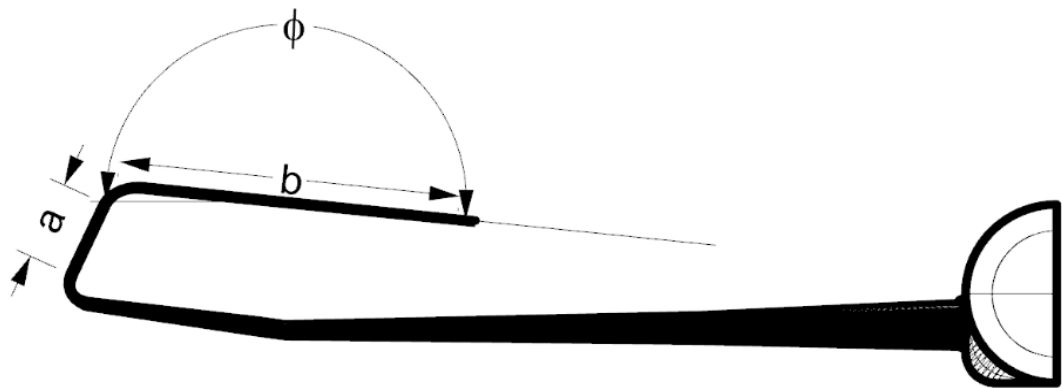
Figure 6.7. Optimization variables for C-wing geometry.

The optimization problem in this study can be defined as:

$$\max{(C_L/C_D)}$$

$$\text{subject to :} \quad g_1(s) = 0.4 < a + b < 0.6$$

$$g_2(s) = C_L > C_{L_{original}}$$

$$\vec{s} = \{a, b, \phi\}$$

$$s_l = \{0.01, 0.40, 90\}$$

$$s_u = \{0.15, 0.70, 220\}$$

For the samples of interest, 25 flow analyses were run and each of the results obtained were saved in a seperate working directory. Considering that each analysis takes an average of 40 minutes, the total calculation time to complete optimization framework has lasted approximately 17-18 hours.

After all simulations were completed, the surrogate model and the response surfaces were created and using the following constraints and bounds optimum geometry was found for three different optimization algorithms.

Table 6.1. Optimization variables under certain constraints.

	$a\ (m)$	$b\ (m)$	$\phi\ (deg)$
Lower Bound	0.0100	0.4000	90.00
Upper Bound	0.1500	0.7000	220.00
Original Values	0.1250	0.5510	186.10
Optimum Values (CGM)	0.0365	0.5634	172.42
Optimum Values (QNM-FDM)	0.0240	0.5759	177.09
Optimum Values (QNM-BFGS)	0.0127	0.5872	182.20

In order to understand the accuracy of surrogate model, three random geometries were created. The flow analyses were performed in STAR CCM+ and compared the results with those of the surrogate model. All results are given in Table 6.3. For C_L, the relative error of the surrogate model is between 2-4% with respect to the high-fidelity solution, while it is calculated as 10% for C_D. High fidelity analysis takes 40 minutes but surrogate model will give the result in only one minute.

Table 6.2. Comparison of the results obtained with high-fidelity flow solver (Star-CCM+) and surrogate model (Kriging method).

		Case I	Case II	Case III
	Parameters $\{a,b,\phi\}$	$\{0.09\ 0.45\ 120\}$	$\{0.12\ 0.65\ 190\}$	$\{0.14\ 0.56\ 210\}$
High-Fidelity Flow Solver	C_L	0.1884	0.1642	0.1750
	C_D	0.0232	0.0242	0.0241
	C_L/C_D	8.1215	6.7867	7.2252
Surrogate Model	C_L	0.1794	0.1659	0.1788
	C_D	0.0187	0.0219	0.0220
	C_L/C_D	9.5935	7.5753	8.1272

Weight of the wing can be restricted by giving an upper and lower limit value for $a + b$ which defines height and length of C-wing tip. It is possible to differentiate this optimization problem by changing this restriction value as desired. Considering the constraints given, the objective function was maximized using QNM-FDM, QNM-BFGS and CGM methods in Dakota. According to Table 6.1, it can be stated that aerodynamic efficiency was increased with the increment in dihedral angle and decrement in the values of a and b parameters. As a result, the values obtained for original and optimum geometries were compared in Table 6.3.

Table 6.3. Aerodynamic forces for optimum and original geometry.

	Original Geometry	Optimum Geometry (CGM)	Optimum Geometry (QNM-FDM)	Optimum Geometry (QNM-BFGS)
C_L	0.1705	0.1708	0.1707	0.1706
C_D	0.0220	0.0216	0.0215	0.0217
C_L/C_D	7.7500	7.9071	7.9395	7.8617

In Figure 6.8, comparison between optimum and original geometries is given using the frontviews and all changes made in the geometry due to optimization process can be examined.
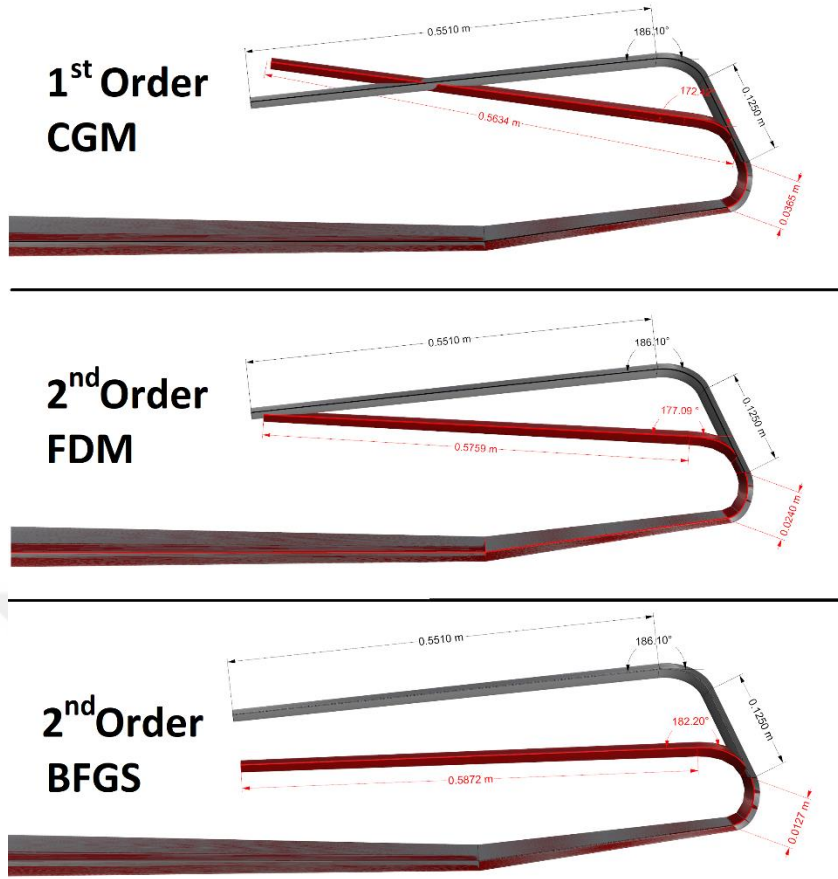
Figure 6.8. Comparison of the original geometry (grey) and optimum geometry (red) in terms of aerodynamic efficiency (C_L/C_D) for three different optimization method.

Figure 6.9 shows the change in objective function depending on the iteration number. Since a gradient-based algorithm which generally provides a quick convergence speed was used, the cost function converged in eight iterations under the given constraints. In this study, the tolerance for relative error between two iterations was given as 10^{-5}. When the relative error calculated reach this value, the optimization process stopped automatically.
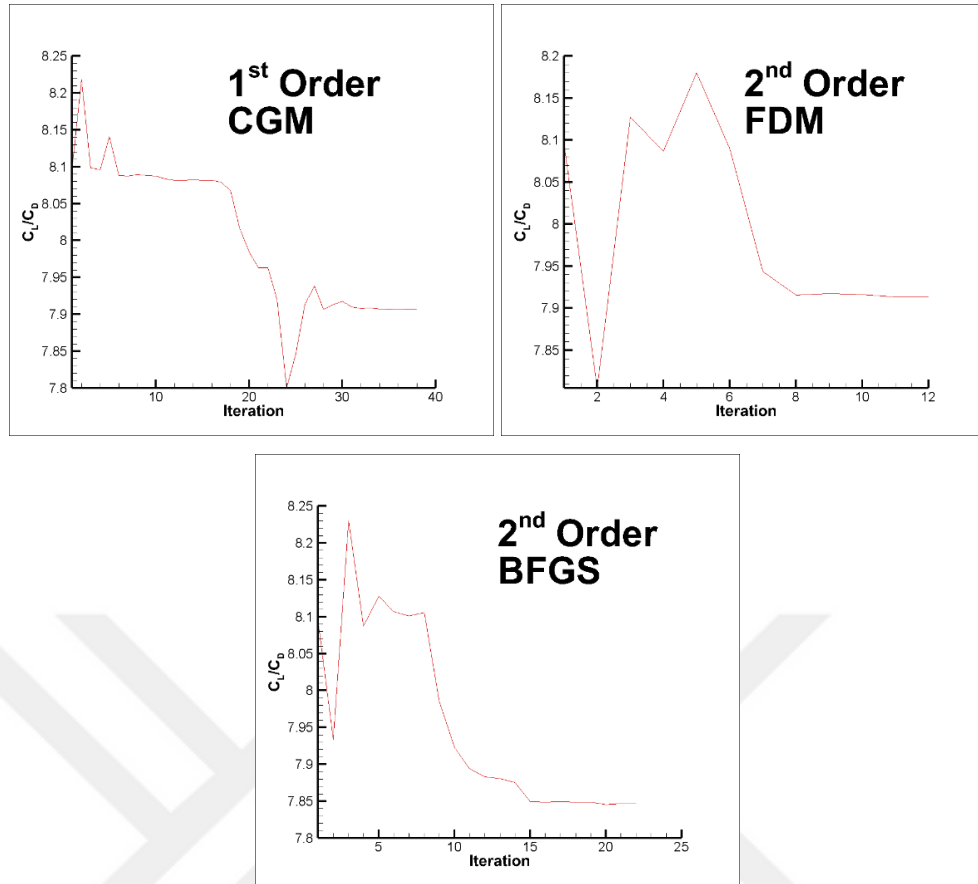
Figure 6.9. Optimization history for each method according to iteration and cost function for 10^{-5} convergence tolerance.

Function evaluation and iteration number of these three optimization method can be found in Table 6.4. It can be said that even though Quasi Newton with FDM did highest function evaluation in three of them, it has the fastest convergence among all.

Table 6.4. Number of function evaluation and iteration number of optimization methods.

|	Number of Function Evaluation	Iteration Number
CGM	98	38
QN (BFGS)	154	22
QN (FDM)	516	12

It is also possible to examine pressure distribution on the aircraft for both original and optimum geometries. Since all optimum geometries have similar pressure distribution only one of them was indicated to make a comparison. According to Table 6.3, Quasi Newton which uses Finite Difference Method to determine Hessian matrix gives the best aerodynamic efficiency.
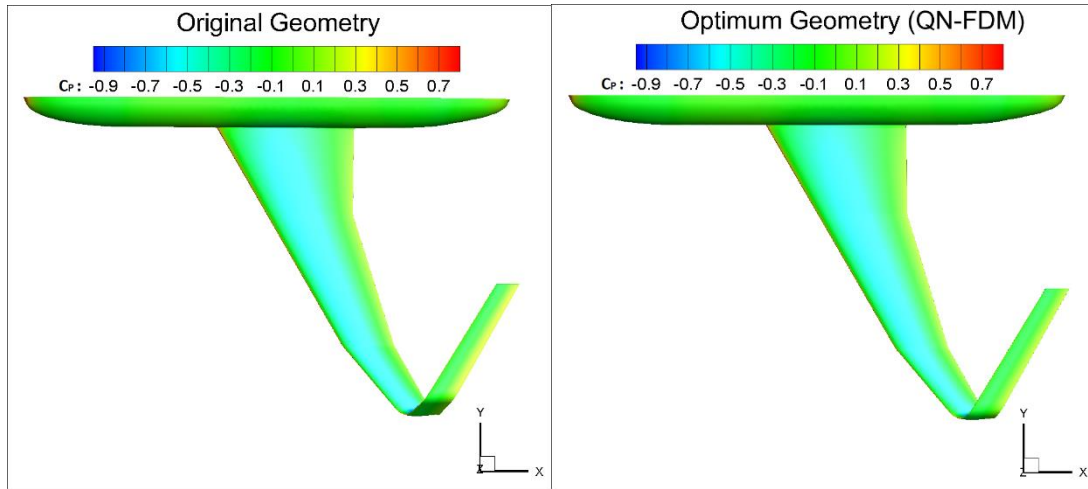
Figure 6.10. Pressure distribution for original geometry and optimum geometry by QN-FDM.

Pressure distributions of the upper side of the geometries can be examined in Figure 6.10. It can be seen that the pressure distribution on the tip side of the original geometry is higher than the optimum geometry. This shows that less lift force will occur on the original geometry compared to optimized wing shape.

As it was explained previously, the design purpose of C-wing configuration is to produce lower induced drag compared to planar wing geometry (see Figure 6.5 and 6.6). After optimum geometry was obtained in terms of aerodynamic efficiency (C_L/C_D), streamtraces for optimum and original geometry were shown in Figure 6.11 and Figure 6.12. Since aerodynamic efficiency was found higher than the other optimization method using QN-FDM approach, only this geometry was compared with the initial C-wing geometry showing the streamtraces. It can be seen that, velocity gradient of the original C-wing geometry is greater than the optimum one on the wing tip. Therefore there will be higher induced drag occured on the original geometry (see Figure 6.11).
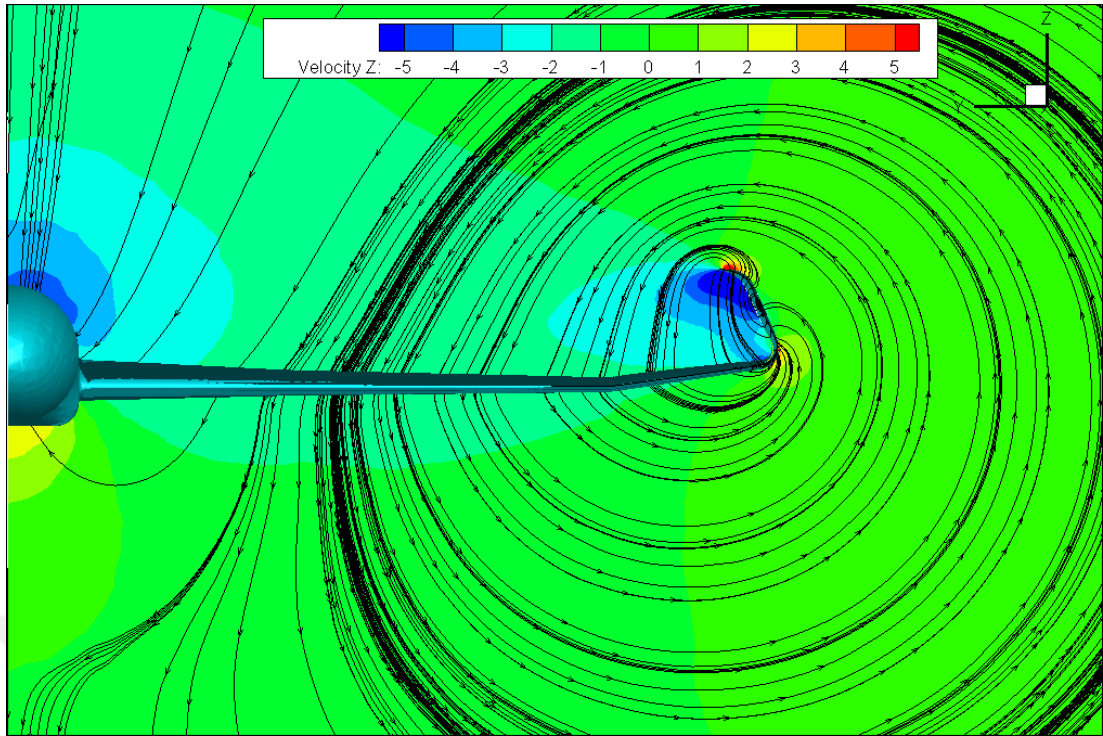
Figure 6.11. Streamtraces for the initial C-wing geometry at zero angle of attack.
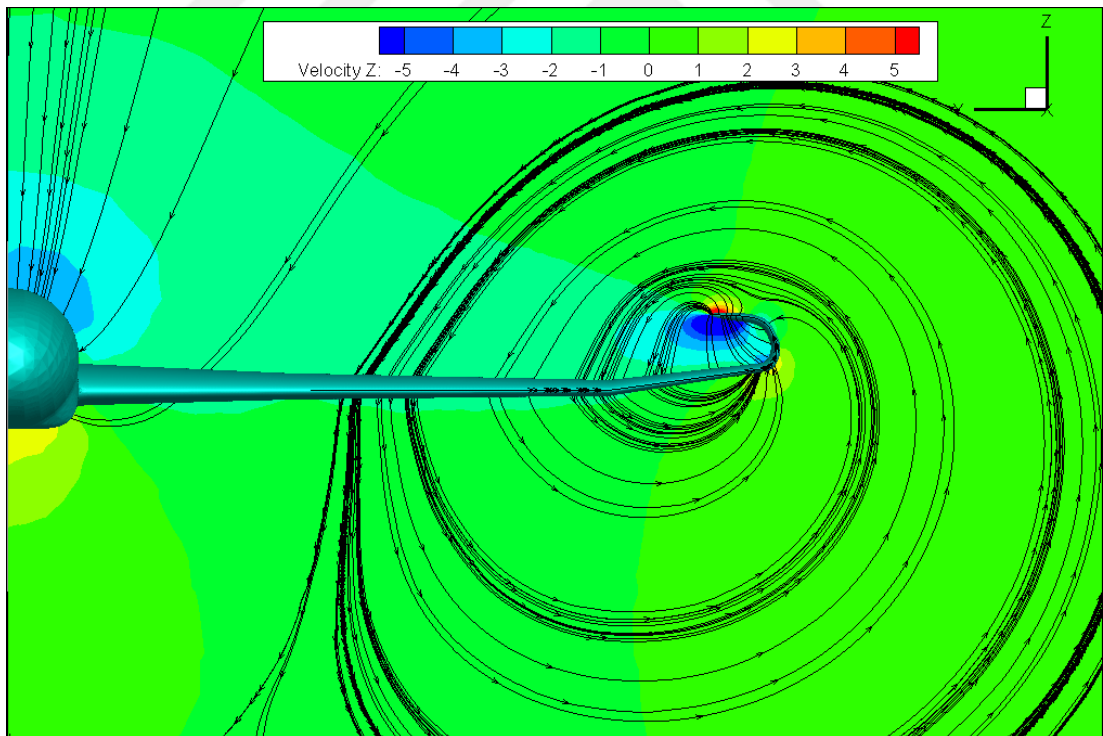
Figure 6.12. Streamtraces for the optimum C-wing geometry (QN-FDM) at zero angle of attack.

7. CONCLUSIONS AND RECOMMENDATIONS

In this study, flow around a C-wing configuration as non-planar wing was numerically investigated and the geometry was optimized to increase aerodynamic efficiency. It was aimed to increase the efficiency as much as possible under certain constraints.

In the first part of study, validation of the numerical model was carried out using experimental data. It was depicted that the physical model of simulations is sufficiently accurate so that the numerical results agree well with the experimental data.

Secondly, optimum geometry for C-wing was investigated to increase aerodynamic efficiency. In this context, an optimization framework was established and multiple tools were integrated into the analysis. Several scripts were developed for these tools to be coupled to each other. Aftere CFD-based optimization framework has been created, optimization problem was defined. Three variables were selected as optimization variables and a sampling study was performed using LHS method with random selection. A surrogate model was created using the sampling results and the optimization process was carried out using these models. Aerodynamic efficiency of the optimized geometry was found to be higher than the original one as we expected, therefore the goal of this study was accomplished.

In the future work, it is planned to perform an optimization study taking into account parameters such as induced drag, wake vortex, static/dynamic stability and it is also aimed that including the effects of aerostructural interactions in the problem.

REFERENCES

[1] Schneider, W., (2001). "The importance of aerodynamics in the development of commercial successful transport aircraft," Page 9-16, Notes on Numerical Fluid Mechanics. Bremen, Springer.

[2] Hicken, J.E., Zingg, D.W., (2010) "Induced-drag minimization of nonplanar geometries based on the Euler equations," AIAA Journal 48, No.11, 2564-2575.

[3] Jansen, P.W., Perez, R.E., Martins, J.R.R.A., (2010), "Aerostructural optimization of nonplanar lifting surfaces," Journal of Aircraft 47, No.5, 1490-1503.

[4] Kroo, I., (2004), "Innovations in Aeronautics," 42nd AIAA Aerospace Sciences Meeting, AIAA 2004-0001, January 5-8, Reno, Nevada.

[5] Skinner, S.N, (2018), "Study of a C-wing Configuration for Passive Drag and Load Alleviation", PhD Thesis, University of Glasgow, June

[6] Andrews, S.A., Perez, R.E, (2018), "Comparison of box-wing and conventional aircraft mission performance using multidisciplinary analysis and optimization", Aerospace Science and Technology, May.

[7] Suresh, C., Paramaguru, V., Ramesh, K." (2015), Aerodynamic performance analysis of a non-planarC-wing using CFD", Aerospace Science and Technology,40, 56-61 October.

[8] Gobpinaath, M., Sivajiraja, K., Suresh, C., Ramesh, K., (2016), " Design and Analysis of Non Planar Wing in Commercial Aircraft", International Journal of Innovations in Engineering and Technology, 2319 − 1058, Vol. 7, Issue 3, October.

[9] Peng, C., Jinglong, H., (2012), "Prediction of flutter characteristics for a transport wing with wingtip devices", Aerospace Science and Technology,23 (1), 461–468.

[10] Demasi, L., Dipace, A., Monegato, G., Cavallaro, R., (2014), "Invariant Formulation for the Minimum Induced Drag Conditions of Nonplanar Wing Systems", AIAA Journal, Vol. 52, No. 10, October

[11] Ning, S.A, Kroo, I., "Tip Extensions, Winglets, and C-wings: Conceptual Design and Optimization", In 26th AIAA Applied Aerodynamics Conference pp. 7052.

[12] Skinner, S.N., Zare-Behtash, H., (2018)," Study of a C-wing configuration for passive drag and load alleviation", Journal of Fluids and Structures 78 175–196.

[13] Kroo, I., 2005, "Nonplanar wing concepts for increased aircraft efficiency," VKI lecture series on Innovative Configurations and Advanced Concepts for Future Civil Aircraft, June 6–10.

[14] Simonsen, C.D., (2000)"Rudder, Propeller and Hull Interaction by RANS", Technical University of Denmark, PhD. Thesis, May.

[15] White, F.M & Corfield, I. (2006). **"**Viscous fluid flow" (Vol. 3, pp. 433-434). New York: McGraw-Hill.

[16] Fletcher, C.A.J., (1991). "Computational Techniques for Fluid dynamics I - Fundamental and General Techniques", Springer-Verlag, Newyork.

[17] Versteeg, H.K., Malalasekera, W. (2007). "An Introduction to Computational Fluid Dynamics", Pearson Education, England.

[18]P.J, Roache, (1998). "Verification and Validation in Computational Science and Engineering", Science and Engineering, Hermosa Publishers, Albuquerque.

[19] F. Stern, R.V. Wilson, H.V. Coleman, E.G. Paterson, (2001). "Comprehensive approach to verification and validation of CFD simulations—part 1: methodology and procedures", J. Fluids Eng. 123 (4) 793–802.

[20]Arora, J.S., (2016). "Introduction to Optimum Design", Elsevier, England.

[21] Armstrong, M., (1998). "Basic Linear Geostatics" Springer-Verlag Berlin Heidelberg, Newyork.

[22]Adams et al. (2018). "Dakota, A Multilevel Parallel Object-Oriented Framework for Design Optimization, Parameter Estimation, Uncertainty Quantification, and Sensitivity Analysis: Version 6.9 User's Manual"

[23] Travis Carrigan Aircraft Mesher Script for Pointwise Retrieved: 01/03/2019 from https://github.com/pointwise/AircraftMesher/blob/master/AircraftMesher.glf

[24] Smagorinsky, J. (1963). "General circulation experiments with the primitive equations: I. The basic experiment". Monthly Weather Review. Vol.91 No. 3, pp. 99-164.

[25] Munk, M., (1921). "Minimum Induced Drag of Airfoils," NACA Rept. 121.

[26] Pointwise (2016). User Guide V18.0R1.

[27] NASA (2014). User Manual OpenVSP V3.17.0.

[28] Cd-Adapco, (2017). User Guide STAR-CCM+ Version 12.02.

[29] Spalart, P., & Allmaras, S. (1992). "A one-equation turbulence model for aerodynamic flows". In 30th aerospace sciences meeting and exhibit (pp. 439).

[30] Deck, S., Duveau, P., d'Espiney, P., & Guillen, P. (2002). "Development and application of Spalart–Allmaras one equation turbulence model to three-dimensional supersonic complex configurations", Aerospace Science and Technology, 6(3), 171-183.

[31] Jones, W. P., & Launder, B. E. (1972). The prediction of laminarization with a two-equation model of turbulence. International journal of heat and mass transfer, 15(2), 301-314.

[32] Launder, B.E., and Sharma, B.I. (1974). "Application of the Energy Dissipation Model of Turbulence to the Calculation of Flow Near a Spinning Disc", Letter in Heat and Mass Transfer, vol. 1, no. 2, pp 131-138.

[33] Menter, F. R. (1994). "Two-Equation Eddy-Viscosity Turbulence Models for Engineering Applications", AIAA Journal, vol. 32, no 8. pp. 1598-1605.

[34] Fock, B. (2014). RANS versus LES models for investigations of the urban climate (Doctoral dissertation, Universität Hamburg, Hamburg).

CURRICULUM VITAE

Name Surname   **:** Hulya SUKAS

Place and Date of Birth   **:** Istanbul 09/01/1994

E-Mail   **: hulyaistifsukas@gmail.com**

EDUCATION   **:**

- **B.Sc.**   **:** 2017, Yıldız Technical University, Naval Architecture
  and Marine Engineering Faculty, Naval Architecture and Marine Engineering

                               : 2018, Yıldız Technical University, Mechanical
  Engineering Faculty, Mechanical Engineering (Double Major)

PROFESSIONAL EXPERIENCE AND REWARDS:

- First class degree in Naval Architecture and Marine Engineering Department

OTHER PUBLICATIONS, PRESENTATIONS AND PATENTS:

- **Sukas, H.**, Kantaroglu, M., Kinaci, O.K. An Adjoint Numerical / Empirical Approach t**o** Predict the Total Resistance of Ships. GMO Journal of Ship and Marine Technology, Vol:23, 208, pp. 31-44.